



PII S0016-7037(00)00597-4

Fractionation trends among IVA iron meteorites: Contrasts with IIIAB trends

J. T. WASSON^{1,2,*} and J. W. RICHARDSON¹¹Institute of Geophysics and Planetary Physics, University of California, Los Angeles, CA 90095-1569, USA²Department of Earth and Space Sciences and Department of Chemistry and Biochemistry, University of California, Los Angeles, CA 90095-1569, USA

(Received April 28, 2000; accepted in revised form October 9, 2000)

Abstract—A neutron-activation study of 48 group-IVA irons shows much lower negative slopes on Ir–Au and Ir–As diagrams than observed in the larger magmatic group IIIAB. This difference seems to reflect the tendency of D_{Ir} , D_{Au} and D_{As} to increase with increasing S content. Contents of S and other volatiles are much lower in IVA irons than IIIAB irons. We show that both groups can be fit with D_X values that depend quadratically on S, with initial IVA S contents about 6X lower than those in IIIAB. The IVA scatter fields show a spread in Au or As at constant Ir that appears to reflect variations in the fraction of trapped melt between 0% and 30%. Copper shows an S-shaped trend that may reflect moderate positive and negative changes in D_{Cu} as the magma evolved or, less likely, sampling variations in a broad band reflecting fractionation and trapping of melt. Gibeon, the largest IVA iron with a mass > 30 tons, shows an appreciable range in compositions consistent either with differences in the degree of magma crystallization or with differences in the content of trapped melt. A striking difference between IVA and IIIAB is observed in the Ir/Au ratios in the most Ir-rich irons in the groups; that in IVA is 40% lower than the IIIAB ratio, and lower than those in other iron-meteorite groups. The IVA Ir/Au ratio is about half the ratios in the chondrite groups. We examined three possible explanations of this anomaly: (1) the high-Ir irons contain large amounts of trapped melt; or (2) half of the IVA core (i.e., the first 50% to crystallize) is missing from the terrestrial set of IVA irons; or (3) the IVA magma formed by incomplete melting of the metal in the chondritic precursor material, with the metal that remained in the mantle having high Ir and low Au contents. Plausibility arguments favor the third possibility. The third scenario is the most plausible, but the second cannot be ruled out. We review recent evidence regarding the cooling rates in group IVA. In contrast to recent interpretations, we note several lines of evidence that indicate constant cooling rates independent of composition, as expected if all IVA meteorites were in the same core when cooling between 900 and 650 K occurred. *Copyright © 2001 Elsevier Science Ltd*

1. INTRODUCTION

Like the large magmatic iron-meteorite group IIIAB, group IVA shows a linear negative trend on log Ir–log Ni diagrams, but the IVA slope is much less steep than the IIIAB slope (Scott, 1972). As discussed by Wasson (1999), sampling and experimental errors for Au and Ni are similar but the total Au range within magmatic groups is several times larger, thus Au is a much better choice than Ni for the independent axis on such diagrams; As is similar to Au in this respect.

Our research team has initiated a program to gather high-precision neutron-activation data on the three large magmatic iron-meteorite groups (IIAB, IIIAB and IVA). We have data for 160 IIIAB irons some of which are reported in Wasson (1999). In this paper we report data for 48 members of group IVA. Although the IVA and IIIAB irons show roughly the same range in Ni contents, the IVA irons are fine octahedrites with bandwidths around 0.3 mm, whereas the IIIAB irons are medium octahedrites with bandwidths around 1 mm. This suggests that the IVA core cooled through the ($\alpha + \gamma$) field ($\alpha =$ kamacite, $\gamma =$ taenite) at a faster rate than the IIIAB core, but some studies (e.g., Rasmussen et al., 1995) suggest a range of IVA cooling rates that correlate with composition and overlap with IIIAB cooling rates.

Another important difference between the IVA and IIIAB initial magma is the lower contents of the most volatile elements (Ga, Ge, Sb) in IVA. The P content appears to have been $\approx 4X$ lower in IVA than in IIIAB (e.g., Scott, 1972), and we suggest that the S content was $\approx 6X$ lower in IVA. The groups also differ in their O-isotopic compositions; IVA silicate compositions are similar to those in L and LL chondrites, with $\Delta^{17}\text{O}$ ($= \delta^{17}\text{O} - 0.52 \cdot \delta^{18}\text{O}$) $\approx 1.2\%$, IIIAB silicates and oxides (chromite, phosphate) have $\Delta^{17}\text{O} \approx -0.2\%$, similar to values in main-group pallasites and HED achondrites (Clayton and Mayeda, 1996). The iron-meteorite $\delta^{18}\text{O}$ values also fall in the same general ranges as those in the related groups.

Our extensive data sets show that, early in the crystallization sequence, the slopes of Ir–Au and Ir–As trends are much lower for the IVA irons than for IIIAB irons. We examine two hypotheses that might account for these differences: (1) The difference could reflect major differences in the solid/liquid element partition coefficients (D values, concentration ratios) resulting from compositional differences, particularly differences in the content of the nonmetals S and P; studies (e.g., Jones and Drake, 1983) have shown that decreasing the S content of a metallic magma causes D_{Ir} , D_{Au} and D_{As} to increase. (2) The difference could reflect a lower efficiency of elemental partitioning reflection associated with the higher cooling rates in IVA compared to IIIAB.

*Author to whom correspondence should be addressed (jtwasson@ucla.edu).

Table 1. Mean compositions of 47 IVA irons and three samples of IVA Gibeon determined by INAA (except Ge by RNAA).

IVA meteorite	Cr μg/g	Co mg/g	Ni mg/g	Cu μg/g	Ga μg/g	Ge μg/g	As μg/g	W μg/g	Re ng/g	Ir μg/g	Pt μg/g	Au μg/g
Allan Hills A78252	85	4.13	93.5	148	2.38	0.138	13.3	0.40	<90	0.385	5.0	2.414
Altonah	117	3.96	83.6	139	2.20	0.123	7.59	0.49	203	1.87	5.3	1.463
Alvord	59	3.8	85.1	121	2.11	0.134	6.50	0.56	247	2.10	5.2	1.435
Bishop Canyon	329	3.92	75.8	156	2.06	0.110	2.92	0.60	345	2.83	5.7	0.777
Bodaibo	186	3.91	78.3	147	2.24	0.111	3.78	0.58	271	2.24	5.7	0.943
Boogaldi	60	4.11	89.6	108	2.38	0.133	11.1	0.42	61	0.635	4.9	2.084
Bristol	139	3.93	79.2	130	2.13	0.124	5.03	0.54	225	1.95	6.0	1.139
Bushmanland	146	4.03	87.6	116	2.23	0.134	9.74	0.45	118	1.10	6.0	1.868
Chinaulta	46	4.23	95.4	130	2.03	0.112	13.9	0.28	<30	0.122	2.8	2.540
Cleburne	72	4.03	88.0	130	2.33	0.137	6.86	0.55	220	1.84	6.7	1.500
Cranberry Plains	32	4.17	94.8	146	2.41	0.120	13.4	0.44	120	0.986	5.5	2.530
Cratheus (1931)	253	3.93	78.3	154	2.20	0.111	4.08	0.59	290	2.43	6.6	0.970
Duchesne	54	4.16	92.8	123	2.12	0.125	13.7	0.33	31	0.403	2.7	2.481
Duel Hill (1854)	34	4.29	104.5	209	2.10	0.111	14.4	0.28	<40	0.362		2.762
Fuzzy Creek	18	4.26	111.3	160	2.19	0.138	13.6	0.29	<40	0.197	2.9	2.678
Gan Gan	23	4.13	91.8	116	2.36		12.1	0.43	117	1.11	5.0	2.216
Harriman (Of)	135	3.94	81.2	128	2.15	0.129	5.21	0.50	200	1.90	5.4	1.198
Hill City	46	4.09	90.4	112	2.29	0.144	10.6	0.41	<40	0.977	4.7	2.130
Huizopa	176	3.89	76.6	156	2.09	0.117	3.40	0.57	298	2.60	5.1	0.842
Jamestown	347	3.83	74.5	133	1.71	0.093	2.00	0.62	388	3.43	7.7	0.605
Kossuth	54	4.14	92.7	122	2.52	0.140	12.2	0.37	120	0.870	5.9	2.250
La Grange	223	3.89	75.7	162	2.07	0.115	3.21	0.60	317	2.72	5.8	0.844
Mantos Blancos	73	4.05	87.8	106	2.32	0.130	9.29	0.43	86	0.877	4.5	1.881
Maria da Fe	412	3.77	74.5	139	1.68		2.16	0.62	468	3.78	7.2	0.615
Maria Elena	338	3.84	75.5	147	1.83	0.096	2.47	0.62	362	3.31	5.5	0.682
Mart	24	4.17	92.9	116	2.27	0.137	12.7	0.37	64	0.716	4.0	2.368
Millarville	10	4.17	93.0	133	2.19	0.144	11.3	0.44	150	1.02		2.430
Mount Sir Charles	133	3.95	82.7	130	2.30	0.126	5.80	0.55	199	1.73	5.0	1.261
Muonionalusta	102	3.96	84.8	113	2.09	0.133	6.48	0.51	191	1.73	5.7	1.408
New Westville	41	4.13	94.1	113	2.40	0.139	14.5	0.30	37	0.490	5.0	2.442
Ningbo	102	3.93	81.3	131	2.16	0.134	5.23	0.57	256	2.15	5.1	1.133
Obernkirchen	532	3.85	76.4	146	1.82	0.092	2.20	0.65	407	3.43	5.9	0.673
Otchinjau	165	3.90	78.3	160	2.09	0.119	4.23	0.69	277	2.46	4.9	0.983
Page City	46	4.22	95.5	122	2.08		14.3	0.23	27	0.324	3.9	2.680
Para de Minas	153	3.96	79.9	147	2.16	0.125	5.04	0.57	276	2.39	5.4	1.105
Rembang	69	4.03	87.3	110	2.29	0.134	8.89	0.46	113	1.16	4.4	1.769
Rica Aventura	88	4.16	91.9	114	2.27	0.138	12.2	0.40	<60	0.373		2.510
San Francisco Mtns	360	3.85	77.3	163	2.10	0.102	3.17	0.63	341	2.81	6.1	0.814
São João Nepomuc.	31	3.89	80.2	162	2.13	0.118	4.95	0.54	322	2.73	5.7	1.057
Seneca Township	86	4.02	84.1	113	2.34	0.124	6.65	0.55	230	1.85	5.8	1.470
Signal Mountain	184	3.89	77.6	145	2.10	0.121	3.70	0.55	271	2.45	5.2	0.913
Smithland	109	4.13	91.1	127	2.26	0.133	13.5	0.37	81	0.843	3.9	2.399
Social Circle	474	3.80	73.2	129	1.69	0.092	2.04	0.60	413	3.57	5.9	0.607
Steinbach	534	4.22	94.0	164	2.27	0.134	12.7	0.43	120	0.798	4.6	2.500
Western Arkansas	322	3.84	76.8	150	1.87	0.100	2.62	0.65	390	3.22	5.9	0.669
Wood's Mountain	88	3.91	82.6	158	2.26	0.143	4.89	0.61	263	2.28	4.5	1.216
Yanhuitlan	572	3.83	75.1	150	1.87	0.105	2.50	0.63	386	3.20	6.6	0.666
Yingde	394	3.81	76.0	149	1.80	0.115	2.44	0.65	361	3.13	6.5	0.663
Gibeon samples												
Gibeon 3761,3758	210	3.85	77.8	169	2.04	0.111	3.46	0.63	285	2.52	5.9	0.882
Gibeon 3777,3762	218	3.88	81.9	166	2.16	0.111	4.63	0.65	281	2.46	5.9	1.038
Namibia 1999	132	3.95	81.2	128	2.02		4.76	0.54	245	2.08	5.9	1.175

2. ANALYTICAL TECHNIQUES AND RESULTS

Thirteen elements (12 plus Fe) were determined by instrumental neutron-activation analysis (INAA) in replicate analyses of 45 iron meteorites; our data for Fe were used for internal normalization. More details are given by Wasson et al. (1988) and Wasson et al. (1998). Concentrations of Ge were determined in most irons on other samples by radiochemical neutron activation analysis (RNAA). Although the INAA data were gathered over a two-decade span, significant improvements in the quality were achieved starting in 1986. As a result, a number of the meteorites were restudied and the recent analy-

ses given double weight in the determination of the mean. In most meteorites we had determined high-precision Ni concentrations by atomic-absorption spectrophotometry. In these cases the presently reported Ni means are calculated treating the previous mean as an additional replicate.

Mean compositions of IVA irons are listed in Table 1, and previously unreported individual analyses carried out in or after 1986 are listed in the Appendix. A few means differ from published values because of minor changes in calibration, minor changes in the weighting of replicates, or (in rare cases) the discovery of arithmetic or copying errors. We estimate relative

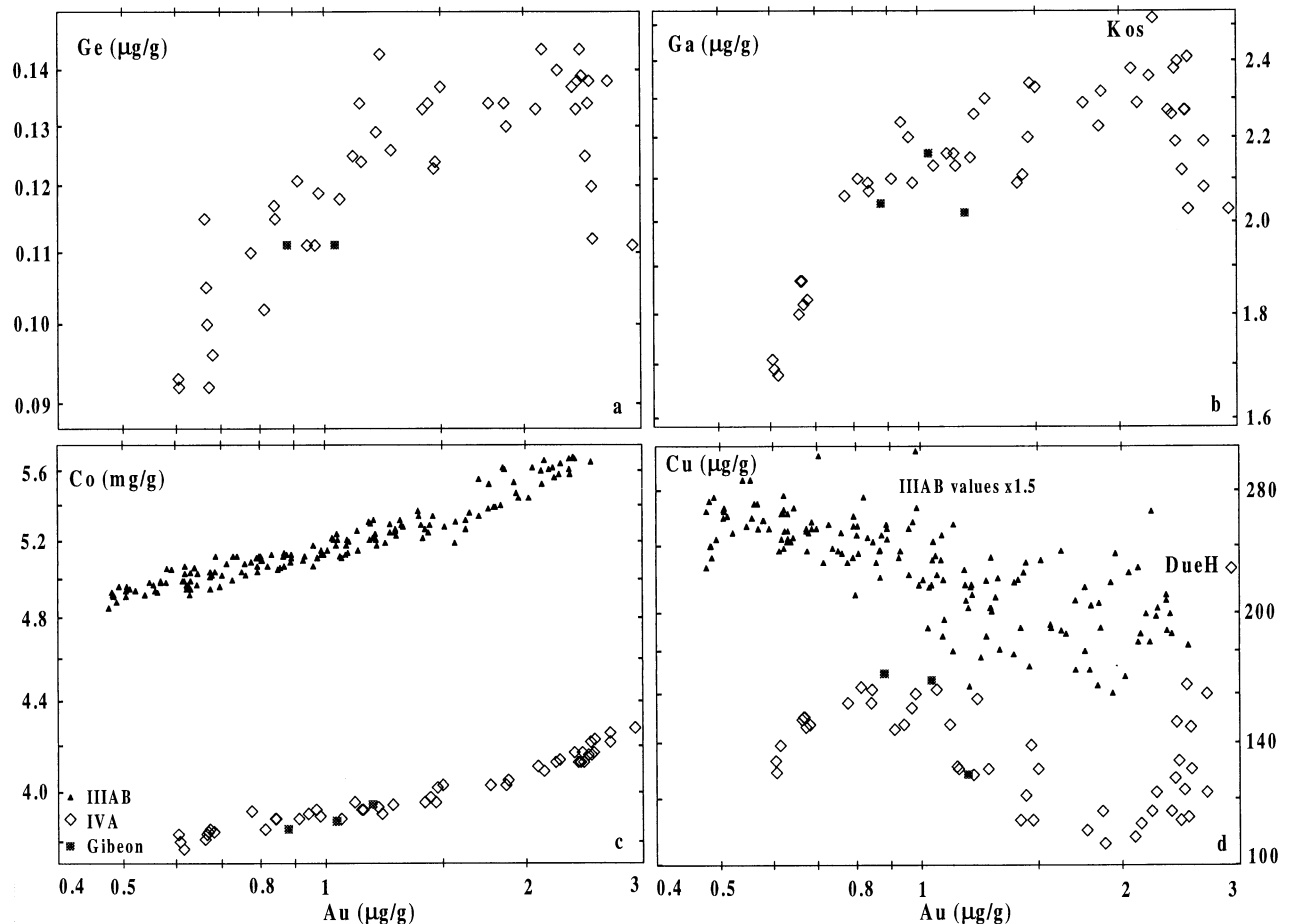


Fig. 1. The taxonomically important elements (a) Ge, (b) Ga, (c) Co and (d) Cu form continuous bands and show relatively small variations among IVA irons. Contents of Co increase continuously with increasing Au, Ge and Ga increase up to a Au content of $2.5 \mu\text{g/g}$, then decrease. The serpentine Cu trend is striking; Cu contents pass through a maximum near $1 \mu\text{g/g}$ Au, then through a minimum at $2.0 \mu\text{g/g}$ before rising sharply. The extreme compositions observed among three members of the Gibeon shower are shown as shaded squares. IIIAB irons form a background cloud of small filled triangles on Figures 1c,d; the IIIAB Cu points are plotted at 1.5X the actual values. Abbreviations: DueH, Duel Hill (1854); Kos, Kossuth.

95% confidence limits to be 2 to 3% for Co, Ni, Ir and Au, 4 to 6% for other elements except Pt, $\approx 10\%$. All Ge and Sb (Table 1) concentrations are previously published RNAA results. There is an Fe interference in the determination of Cr, the result of the $^{54}\text{Fe}(n,\alpha)^{51}\text{Cr}$ fast-neutron reaction (Wasson et al., 1999). The lowest Cr contents we report are $10 \mu\text{g/g}$; this provides an upper limit on the apparent Cr content resulting from fast neutrons on Fe. Our best estimate of the level of interference is $6 \mu\text{g/g}$ Cr per g of Fe. Our data are not corrected for this interference.

3. COMPOSITIONAL CHARACTER OF GROUP IVA IRONS

Our IVA data are plotted on 10 log-log element-Au diagrams in Figures 1 and 2. In those cases where group IIIAB irons occupy the same general space (all except Figs. 1a,b, the Ga-Au and Ge-Au diagrams) these are plotted as a background cloud of filled triangles. The extreme compositions found in the IVA Gibeon shower are shown as separate symbols (shaded

squares). As mentioned in the Introduction, there is considerable advantage to choosing Au as the independent parameter rather than Ni, which was used in IVA summary diagrams by Malvin et al. (1984) and Scott et al. (1996). As noted by Wasson (1999), Au is determined with a high precision (relative 95% confidence interval about $\pm 3\%$), at least as good as that for Ni, but the total Au range is much greater (e.g., a maximum/minimum ratio among IVA irons of 5 for Au, 1.6 for Ni).

The first four diagrams (Fig. 1) show elements that are taxonomically useful because their range within the groups is small compared to the range through all irons. The most important of these are Ga and Ge, for which IVA values are so much lower than those in IIIAB that it was not practical to show IIIAB points (Figs. 1a,b). In group IVA both Ga and Ge initially increase rapidly with increasing Au, reach a maximum at $\approx 2.3 \mu\text{mg/g}$ Au, then decrease with increasing Au during the remainder of the group. If we employ the model discussed below, a concentration of $2.3 \mu\text{g/g}$ roughly corresponds to

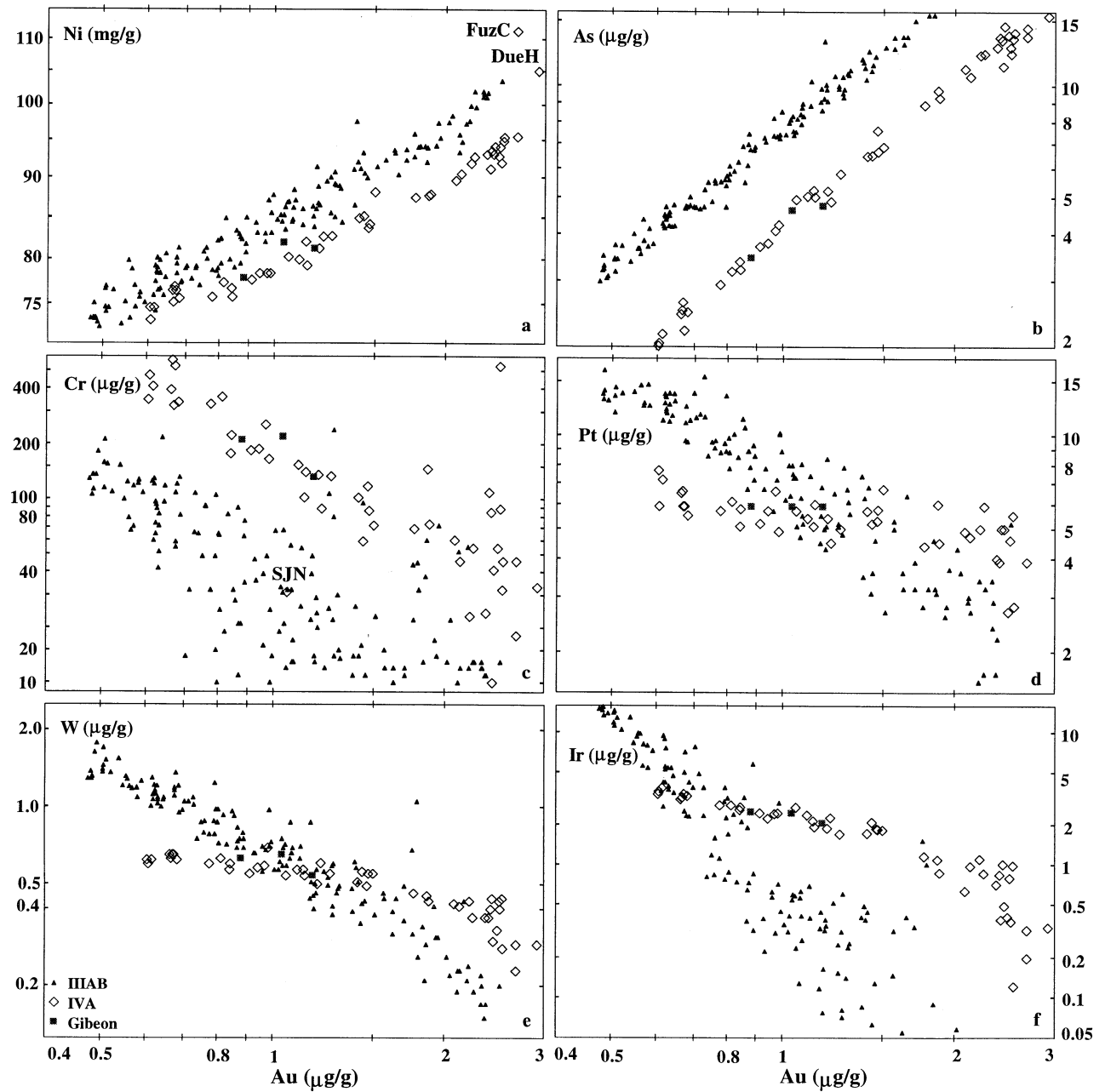


Fig. 2. The elements Ni, As, Cr, W, Pt, and Ir also form continuous bands among IVA irons. As discussed in more detail in the text, IVA seems to be a well sampled core, with only one minor hiatus near $1.7 \mu\text{g/g}$ Au. The compatible elements Ni and As form positive trends with Au, linear except for a sharp increase in Ni in the two irons having the highest Au contents. The negative slopes of the W-Au and Ir-Au trends become more steep with increasing Au content, with most of the increase occurring at Au contents $> 1.7 \mu\text{g/g}$. As in Figure 1, IIIAB irons are shown as a background cloud and the three members of the Gibeon shower as shaded squares. Abbreviations: DueH, Duel Hill (1854); FuzC, Fuzzy Creek; SJN, São João Nepumuceno.

about 80% crystallization of the IVA magma. Note the smaller vertical extent of the scatter field on the Ga-Au diagram, a reflection of the fact that our INAA precision for Ga at $2 \mu\text{g/g}$ is about $2\times$ better than our RNAA precision for Ge at $0.1 \mu\text{g/g}$.

The small vertical spread on the Co-Au diagram (Fig. 1c) demonstrates our high precision for Co. The greatest spread is in the five points near $1.5 \mu\text{g/g}$. We estimate that a 95%-confidence range for our Co means is $\approx 3\%$ relative. Note that

the IIIAB and IVA bands on the Co-Au diagram are essentially parallel, and offset by a factor of about 1.3. The slope of the IVA band increases slightly at Au contents $\geq 1.6 \mu\text{g/g}$; we suggest that this mainly reflects a minor increase in D_{Au} at higher nonmetal contents of the cooling magma, whereas D_{Co} is less affected by this compositional change.

The Cu-Au scatter field (Fig. 1d) is the most remarkable in our IVA compositional study. Because there is extensive over-

lap of the IIIAB and IVA fields we multiplied the IIIAB values by 1.5 before plotting them. The IVA Cu-Au band passes through a maximum at $\approx 1 \mu\text{g/g}$ Au and a minimum at $\approx 2 \mu\text{g/g}$ Au before climbing to the highest Cu values in Duel Hill (1854). There is a hint of similar variations in the downward-trending IIIAB cloud, but there is too much scatter to confidently define peaks or valleys.

In Figure 2 we compare the IVA and IIIAB data on plots of As, Ni, Cr, W, Pt, and Ir against Au. The Ni-Au trend (Fig. 2a) shows a distinct increase in slope with increasing Au even if one neglects the two high-Au irons Duel Hill (1854) and Fuzzy Creek, whose Ni contents plot well above a smooth curve through the other high-Au IVA irons. The IIIAB irons show an essentially linear trend with a slightly higher mean slope; at the low-Au extreme the two groups partially overlap, but (if Duel Hill and Fuzzy Creek are ignored) they are resolved at the high-Au extremes.

The IVA and IIIAB As-Au trends (Fig. 2b) are essentially linear and parallel; regression lines through the two (log-log) data sets have slopes of 1.29 and 1.22, respectively. The two curves differ by a factor of 2 in As at low Au contents (e.g., $\approx 0.7 \mu\text{g/g}$). As discussed in more detail in the following section, the initial $D_{\text{As}}/D_{\text{Au}}$ ratio is lower in IVA than IIIAB; this difference accounts for about half of the offset between the two fields. It is important to note that the very wide range in IVA As contents (a maximum/minimum ratio of 7, higher than the factor of 6 observed in IIIAB) constitutes strong evidence that the set of IVA samples represents a wide range of degrees of crystallization of the IVA core; as discussed below, these appear to range from 0 to 85% crystallization.

The Cr-Au distributions (Fig. 2c) in IVA and IIIAB are similar, but there is more vertical spread in Cr among the IIIAB irons. Much of the scatter reflects the fact that Cr is not a true siderophile, but forms its own phases CrN (carlsbergite), FeCr_2O_4 (chromite), FeCr_2S_4 (daubreelite) which generally exsolved at relatively high temperatures, perhaps within 200 K of the solidus of the metallic magma. Both daubreelite and chromite are common in IVA irons (and often associated with FeS) but, perhaps reflecting a low bulk N content, carlsbergite has not been reported (Buchwald, 1975). The Cr-Au fields for both groups show a downward trend on the Cr-Au diagram implying that D_{Cr} is >1 , even though laboratory studies consistently yield D_{Cr} values ≈ 0.5 at low S contents, and the few data at higher S contents indicate that, in contrast to siderophiles, D_{Cr} decreases with increasing S (Jones and Malvin, 1990). Because the S content of group IVA is less than in IIIAB, this effect may account for a part of the difference between the higher IVA initial Cr contents and the lower IIIAB values. Even allowing for this difference, in the *Mean Elemental Abundances* section we estimate that the Ni-normalized IVA Cr abundance is $\approx 2.5\times$ higher than the IIIAB abundance.

Wasson et al. (1999) reviewed possible models to account for the curious negative trend on the IIIAB Cr-Au diagram, the opposite of that expected if $D_{\text{Cr}} \approx 0.5$. They noted that most Cr is in minor phases, and favored the interpretation that the downward trend reflected a sampling bias on the part of the analysts who avoided samples with visible inclusions. They suggested that, as the whole-rock Cr content increased, the nucleation of chromite that would grow to mm dimensions

occurred at ever higher temperatures, and thus that diffusion from the metal to the chromite became more efficient with increasing degree of crystallization. They stated that the high degree of scatter in Cr contents observed in high-Au IIIAB irons provided support for the view that Cr contents mainly reflect stochastic differences in the sampling of chromite at Au contents $> 0.7 \mu\text{g/g}$ (Fig. 2c). At Au $> 1 \mu\text{g/g}$ there is also much scatter in the Cr contents of IVA irons (Fig. 2c).

Perhaps the most striking differences between IVA and IIIAB trends is observed in the diagrams for the three compatible (and refractory) elements Ir, W and Pt. In each case the absolute values of the negative slopes are substantially lower in IVA than in IIIAB (Figs. 2d,e,f). We discuss and model Ir-Au and Ir-As trends in more detail a later section. There seems to be only one plausible explanation of the lower slopes in IVA compared to IIIAB: initial D values of these elements in the IVA magma were much closer to unity than those in the IIIAB magma, a reflection of the strong dependence of D_{Ir} , D_{Pt} and D_{W} on the nonmetal concentrations in the magma.

Key questions concerning the evolution and history of group IVA are why the Ir range is so small, and whether this small range (and the lower initial Ir/Au ratio in IVA compared to IIIAB) might indicate that an early-crystallized portion of the group is missing. Our data, which show larger As and Au ranges in IVA than in IIIAB, imply extensive sampling of all levels of the IVA core and, as discussed in more detail in the *Mean Elemental Abundances* section, we tentatively endorse the view that IVA irons with the highest Ir contents (e.g., Maria da Fe) represent the first few % of crystallized IVA solids.

4. FRACTIONATION AMONG IVA GIBEON SPECIMENS

At 60 tons, IVB Hoba is the largest individual meteorite in the world. The mass of Gibeon listed in Graham et al. (1985) is 24 tons, but many large masses have recently come onto the market, and J. Koblitz (personal communication) estimates that the total mass is ≥ 34 tons. We suggest that the mass of Gibeon now in public and private meteorite collections is comparable to that of Hoba. The largest amount of Gibeon in one place is a large pile in a public park in Windhoek, Namibia. During a visit to the site Buchwald (1975) counted ≈ 33 individuals weighing ~ 11 tons; he was allowed to remove small research samples.

In an unpublished collaborative study by Buchwald, D. J. Malvin and Wasson in 1980 to 81, compositional data were obtained for 10 samples from the Windhoek Pile. These showed small but seemingly resolvable ranges in Ir, Au and As. To confirm these we reanalyzed pairs of the most extreme samples; our low-Au pair ($0.88 \mu\text{g/g}$ Au) carried Buchwald specimen numbers of 3758 and 3761, the high-Au ($1.04 \mu\text{g/g}$ Au) pair the numbers 3762 and 3777.

We recently received at UCLA a 15-kg IVA iron from Namibia that may also be from the Gibeon strewn field; an exact provenance is not available. We tentatively designate this iron Namibia 1999. If it is a part of the Gibeon shower, it extends the compositional range to an appreciably higher Au content of $1.17 \mu\text{g/g}$, for a maximum/minimum ratio of $1.17/0.88 = 1.33$.

The three Gibeon irons are assigned distinct symbols on

Figures 1 and 2. On all diagrams these plot within the main IVA scatter field. And, on all diagrams, the trend of the three points is roughly parallel to the trend of the main field. If we assume that they formed by fractional crystallization, and use the model discussed in the *Modeling Trends* section, the extreme Au contents in the two Windhoek-pile pairs correspond to 44 and 56% crystallization of the core; the Namibia iron extends the latter value to 62%.

The key question is why Gibeon shows such a large range. The three main scenarios are: (1) that the dimensions of the meteoroid encompassed a sizable fraction of the size of the IVA magma chamber; or (2) that the meteoroid encompassed a sizable fraction of a magma pocket, for example one formed by collapse of the ceiling of the main chamber or by the fusion of giant dendrites à la Haack and Scott (1992) or; (3) that the meteoroid contained variable amounts of trapped melt, a model used by Esbensen et al. (1982) and Wasson (1999) to account for the still larger compositional range in the Cape York IIIAB iron.

Even though Gibeon is an extremely large shower, presumably produced by a highly oblique entry into the Earth's atmosphere, it is difficult to disrupt irons having diameters larger than ≈ 40 m during atmospheric passage (Hills and Goda, 1998). A meteoroid larger than 40 m should produce a crater having a diameter >200 m, large enough to be recognizable today, ≈ 100 ka after Gibeon fell (K. Nishiizumi, pers. comm., 2000). Thus, if Gibeon corresponds to a range of crystallization of $\approx 12\%$, a rough upper limit on the magma body is $8\times$ the meteoroid diameter, <300 m. This seems too small for an asteroidal core that produces such a large present-day terrestrial flux >400 Ma (the common IVA cosmic-ray age) after the breakup event. And if we use the 18% range, the estimated core diameter falls to 200 m. We therefore reject the first scenario.

If the range in Gibeon resulted from fractional crystallization, it seems more likely that the dimensions of the magma chamber were much smaller than those of the core; this sub-chamber probably consisted of a mechanically isolated magma pocket, perhaps formed by the collapse of roof pendants (Esbensen et al., 1982) or by the fusion of dendrite-like columns of solids (Haack and Scott, 1992).

Esbensen et al. (1982) and Wasson (1999) showed that the IIIAB Cape York compositional trends (e.g., a low Ir-Au slope) are consistent with a trapped-melt model but not with the steep slopes expected from a fractional crystallization of a magma pocket. Because of the low slopes on the IVA fields on Ir-Au and related diagrams, it is more difficult to resolve trapped-melt and fractional crystallization scenarios in group IVA as a whole or in Gibeon. It should be possible, however, to resolve these possibilities by (a) obtaining more precise data on the Gibeon trend, and (b) obtaining INAA compositional data on large (>200 cm²) Gibeon sections for which S contents have been determined by point counting. The trapped-melt model predicts contents of FeS should be appreciably ($>2\times$) higher in the high-Au Gibeon irons relative to the low-Au irons. If the range in Au and other elements is the result of fractional crystallization then the FeS content is not expected to correlate with composition, and detailed INAA data should show steeper Ir-Au trends.

5. PUBLISHED IDEAS REGARDING THE FORMATION OF IVA IRONS

The first report of an appreciable (factor of 20) range in cooling rates in group IVA was by Goldstein and Short (1967), based on a calculated relationship between kamacite bandwidth and the bulk Ni content. Schaudy et al. (1972) noted that the compositional data for group IVA were those expected from the fractional crystallization of a metallic magma and that, because of the much higher thermal diffusivity in metal compared to silicate, models in which the magma (core) were surrounded by silicates predict constant cooling rates.

To account for a variation in kamacite bandwidth that appeared to be discontinuous, as well as some of the cooling rate variations and for a small hiatus in Ni contents (between 84 and 88 $\mu\text{g/g}$), Schaudy et al. (1972) suggested that IVA irons might have formed in two different parent bodies. They also suggested the alternative possibility that an impact resulted in the simultaneous nucleation of kamacite throughout the core (or cores), and that this could explain much of the apparent variation in cooling rates.

Rasmussen et al. (1995) carried out the most recent reinvestigation of the IVA metallographic cooling rates, and again inferred a range from ≈ 3000 to ≈ 30 K/Ma, a factor of 100 range. As with past studies showing large ranges in cooling rates, the cooling rates correlate with composition. They suggested that a breakup-reassembly model (Haack et al., 1996; Scott et al., 1996) with 5 of the reassembled fragments of the asteroid contributing IVA irons having different cooling rates could account for this range of cooling rates; they recognized, however, that this did not explain why the inferred cooling rates correlate with composition.

Haack et al. (1996) studied the disordered clinopyroxene in the silicate-bearing IVA irons Steinbach and São João Nepumuceno, and interpreted these to require extremely fast (>100 K/h) cooling rates in the temperature range 1470 to 970 K, but metallographically inferred cooling rates of ca. 1000 K/Ma or less at temperatures below 970 K. They suggested that an asteroidal breakup and reassembly model could account for these very different thermal inertia regimes.

Scott et al. (1996) modeled the crystallization of the IVA core. They estimated the initial S content of the IVA magma to be 25 mg/g, and argued for a jump in D_S from normal values <0.01 to values of ≈ 0.2 at S contents >60 mg/g. They concluded that the low contents of volatiles in IVA were inherited from the chondritic precursor, and not the result of the loss of volatiles following an impact-heating event.

6. THE NUMBER OF IVA PARENT BODIES

Schaudy et al. (1972) suggested that formation of IVA irons in two different parent bodies could account for an apparent hiatus in Ni contents, one that occurred together with an offset in kamacite bandwidth. Our more extensive and somewhat more precise compositional data also show a small Au "hiatus" (at 1.50–1.77 $\mu\text{g/g}$), but there is no hiatus in Ni occurring between the same sets of IVA irons. Figure 3 is a plot of Buchwald's (1975) kamacite bandwidths vs. log Au. Bandwidths are essentially constant at ≈ 0.28 mm until 1.5 $\mu\text{g/g}$ Au; following the compositional hiatus, at ≥ 1.8 $\mu\text{g/g}$ Au bandwidths increase by 40% to a mean value of ≈ 0.38 mm. Because

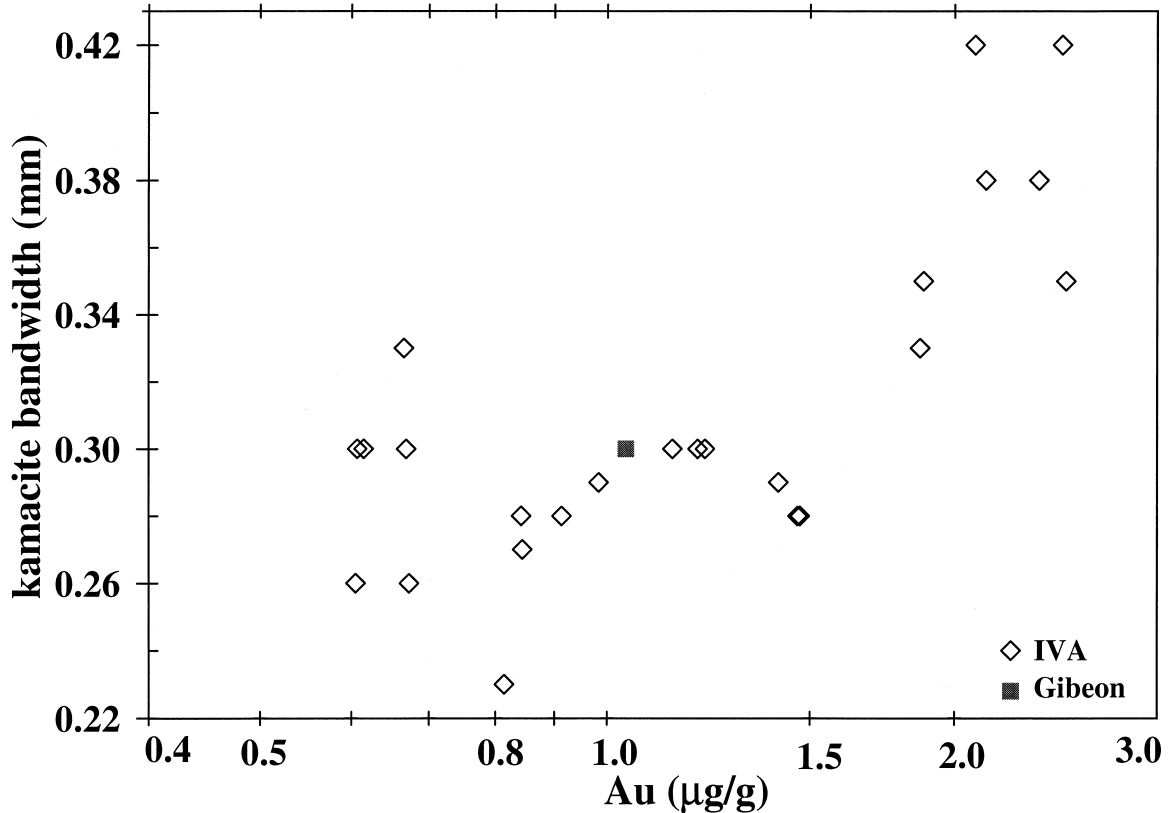


Fig. 3. Kamacite bandwidth increases (by a factor of ≈ 1.5) with increasing Au (and Ni) content in group IVA. The data are consistent either with a discontinuous increase above 1.8 mg/g Au or with a generally positive trend (and, possibly an increase in the slope at the highest Au contents). The latter, which seems more plausible, suggests a model in which the density of crystallization nuclei decreased with increasing Au content.

of the high degree of scatter it is not possible to state whether there is a discontinuous jump above the hiatus or whether the slope is continuously positive, perhaps even increasing at the high Au contents. A monotonic increase seems more plausible in which case the true range would seem to be from ≈ 0.26 to ≈ 0.40 mm.

Because our extensive compositional data set shows all trends to be continuous across the small Au hiatus, we conclude that the IVA irons must originate in a single parent body core. Possible explanations for the distribution of bandwidths are discussed in the following section.

7. FACTORS THAT COULD PRODUCE THE CORRELATION BETWEEN COOLING RATE AND COMPOSITION

7.1. Variable, Composition-Dependent Cooling Rates in Group IVA?

With the exception of the study by Willis and Wasson (1978a), all attempts to use the detailed distribution of Ni between kamacite and taenite or to account for the widths of kamacite lamellae have yielded inferred IVA cooling rates that range over factors of 20 to 100 and correlate with chemical composition. The most recent study by Rasmussen et al. (1995) is typical; Figure 4 shows their estimated cooling rates plotted against Au. Yingde is the point with high cooling rate (3400

K/Ma) and low Au content. The remaining data form two loose clusters, the lower of which scatter about a mean rate of 30 K/Ma. The clusters are separated by the hiatus in IVA Au contents noted above.

As discussed by numerous researchers (e.g., Haack and Scott, 1992), the thermal gradient across a solid asteroidal core is very small. The reasons are: (1) the thermal conductivity in metal is $30\times$ higher than in the surrounding silicates; and (2) there is no heat source in the solid core. For that reason a factor of 100 range in cooling rates is grossly inconsistent with storage in the same core when temperatures were in the range 650 to 850 K.

Rasmussen et al. (1995) and Haack et al. (1996) agreed that one parent body best accounted for the compositional data and the clustering in cosmic-ray ages, but suggested that the cooling-rate data could be explained by a catastrophic breakup of this core followed by reassembly. Following this event the IVA irons were located in 5 distinct cooling environments. A major problem with this interpretation is the miraculous manner in which 5 pieces of the fragmented core were reassembled with a wide range of thicknesses of the overlying insulating silicates correlated with the compositions of the metallic fragments below these layers.

If the cooling rate clusters each showed wide and overlapping ranges in composition, it might be reasonable that the

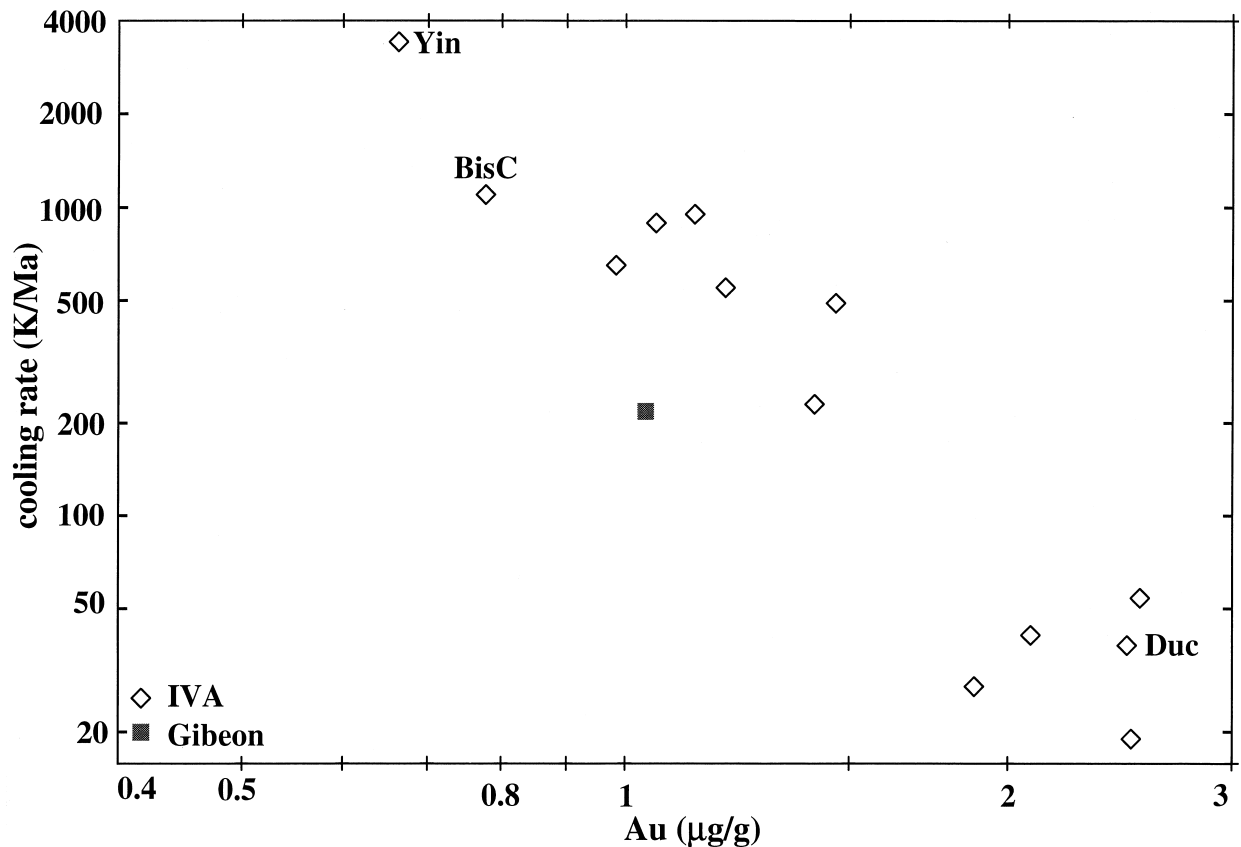


Fig. 4. Cooling rates inferred for IVA irons correlate with composition, as shown in this log-log plot of cooling rates (Rasmussen et al., 1995) vs. Au. Estimated cooling rates decrease by a factor of ≈ 100 as Au increases by a factor of 5. We suggest that these systematic effects are artefacts largely resulting both from small errors in phase diagrams and diffusion coefficients, erroneously high P contents of low-Au irons, and other factors mentioned in the text. Abbreviations: BisC, Bishop Canyon; Duc, Duchesne; Yin, Yingde.

cooling rate differences reflect differences in insulation in a fragmented and reassembled parent body. However, in our view, the correlation with composition strongly implies a systematic error in the model used to infer the cooling rates from the compositional/structural observations.

Cooling rate protocols involve the use of low-temperature phase equilibria and diffusion coefficients, both of which are poorly constrained because diffusion is such a slow process in the relevant temperature regime, roughly 650 to 850 K. For example, the diffusion coefficient in P-free kamacite is $10^{-17} \text{ cm}^2 \text{ s}^{-1}$ at $\approx 800 \text{ K}$ (Dean and Goldstein, 1986), thus laboratory experiments with durations of 10^7 s produce diffusion lengths ($= D \cdot t^{1/2}$) of $10^{-5} \text{ cm} = 0.1 \mu\text{m}$. Complicating the situation is the fact that both the phase equilibria (mainly the $\alpha/(\alpha + \gamma)$ boundary) and the diffusion coefficients are affected by the nonmetal content of the system, particularly P and C. The effect of C is not well defined, but increasing P has the effect of decreasing the Ni content of the $\alpha/(\alpha + \gamma)$ boundary (Moren and Goldstein, 1979; Saikumar and Goldstein, 1988) and increasing the diffusion coefficients of Fe and Ni in α and γ at constant T (Dean and Goldstein, 1986).

Willis and Wasson (1978a) took the approach that, because the compositional and cosmic-ray-age data strongly indicated that IVA had formed in a single fractionally crystallized core,

one should examine whether the uncertainties in phase boundaries and diffusion coefficients would permit constant cooling rates within IVA. Using trial and error techniques they increased the curvature of the $\alpha/(\alpha + \gamma)$ boundary, and showed that their diagram (which is similar to that of Romig and Goldstein, 1980) and plausible diffusion-coefficient relationships were able to produce constant cooling rates of about 25 K/Ma. They used the Ni diffusion coefficients in kamacite and taenite by Hirano et al. (1961), in part because data were obtained at lower temperatures than in other studies, but also because these, after making plausible adjustments for the effect of P, allowed taenite central Ni values to be matched with essentially constant cooling rates, independent of composition. Moren and Goldstein (1978) argued that the diffusion data used by Willis and Wasson (1978a) were not as good as those extrapolated from data obtained at higher temperatures by other research groups, but did not evaluate the merits of the Willis-Wasson approach (i.e., to adjust parameters within experimental limits to minimize variations in cooling rate).

Willis and Wasson (1978b) countered the critiques of Moren and Goldstein (1978), and called attention to two other indicators that implied near-constant cooling rates across the composition spectrum of IVA irons: high-Ni (high-Au) and low-Ni (low-Au) IVA irons (1) have similar taenite Ni values mea-

sured at the interface with kamacite, and (2) show similar kamacite profiles. Both of these should be resolvably different if cooling rates in the high-Ni IVA irons were really $\geq 30\times$ lower than at the low-Ni extreme of the group.

Another recent indication of constant cooling rates in IVA is the island size in cloudy taenite. Taenite lamellae that are wide enough to have Ni contents $\leq 30\%$ in the centers consist of martensitic mixtures in these central regions, clear taenite at the border to kamacite, and cloudy taenite between the clear taenite and the martensite. Yang et al. (1997) noted that high-magnification images show that cloudy taenite consists of islands of taenite in a matrix of kamacite, and that the logarithm of the mean island width (IW) near the border to clear taenite is inversely correlated with log cooling rate (CR) inferred via other metallographic techniques. A rough fit of the trend through their figure 5 yields the relationship: $\log CR = -2.14 \log IW + 5.14$. The advantage of this technique is that the cloudy zone forms at such a low temperature (≈ 670 K) that schreibersite will have nucleated in all irons with the possible exceptions of those having very low P contents (possibly including the low-Au extreme of IVA). Their data yield mean island widths of $53.8 \pm 5.1 \mu\text{m}$ in 4 IIIAB irons and 28.2 ± 8.0 in 6 IVA irons, with no evidence of a compositional dependence in either group. On the basis of the above relationship we calculate mean cooling rates of 27 K/Ma in IIIAB and 109 K/Ma in IVA. Because of the relatively unsophisticated level to which the method has been developed the absolute values may have large errors, but we suggest that the factor of 4 difference in cooling rates between IIIAB and IVA is the best estimate of the difference between these groups currently available.

K. L. Rasmussen (pers. communication, 2000) has kindly provided some new cooling rate simulations based on the lower P contents that, in the following section, we suggest to be appropriate to low-Ni-IVA irons. These resulted in a cooling rate of Bishop Canyon of 600 K/Ma, $\approx 2\times$ lower than that reported by Rasmussen et al. (1995). Thus, insertion of correct P values into the Rasmussen algorithm reduces the cooling-rate range from Bishop Canyon to Duchesne from a factor of ≈ 30 to a factor of ≈ 15 , still a very high range.

The Rasmussen algorithm proved unable to reproduce the closely similar kamacite profiles in low-Ni and high-Ni irons reported by Willis and Wasson (1978b) and Moren and Goldstein (1978). Although simulations at a cooling rate of 38 K/Ma roughly reproduce the near-constant Ni content of ≈ 74 mg/g observed by Willis and Wasson (1978b) in the high-Ni iron Hill City, calculations at 1100 K/Ma for a low-Ni IVA composition yielded Ni contents that are too low. In particular, the simulated Ni content of Bishop Canyon kamacite never exceeds 65 mg/g, and is < 60 mg/g at distances $> 20 \mu\text{m}$ from the interface with taenite whereas the Willis-Wasson kamacite data for Gibeon and Signal Mountain $> 20 \mu\text{m}$ from the interface are essentially the same at ≈ 73 mg/g.

There is thus ample reason to feel that improvements are still needed in the cooling rate algorithm, and to keep an open mind regarding the reported correlation between cooling rate and composition. One factor not included in past simulations that could play a role is a possible difference in nucleation mechanism for low-P and high-P irons; if the ideas of Reisener and Goldstein (2000) are correct, kamacite nucleation in low-Ni IVA irons may occur at $T < 750$ K by the diffusionless mar-

tenitic transition, whereas that in the P-saturated high-Ni IVA irons may occur at $T > 850$ K, either by homogeneous-nucleation or precipitation on phosphides.

7.2. P Concentrations in IVA Irons

We noted above that the P contents used by Rasmussen et al. (1995) for low-Ni IVA irons are systematically high. Because there are no visible phosphides in many low-Au IVA irons Buchwald (1975) could only give upper limits based on rough estimates of the P dissolved in the kamacite. Unfortunately, some of these upper limits were transcribed as real values in Buchwald's Appendix I.

Until more determinations become available, we suggest that one can obtain precise P estimates by taking advantage of the close geochemical relationship between P and As. These two elements behave similarly during fractional crystallization of metallic magmas, with D_P slightly lower than D_{As} . The close relationship is underscored by the fact that, at low temperatures, both elements partition into kamacite, in contrast to most other siderophiles.

In Figure 5 we show how this approach would work: P is plotted against As for IIIAB and IVA. With two exceptions, all P data are from Moore et al. (1969) and Lewis and Moore (1971), who used a milling technique in an attempt to obtain representative sampling of all phases. The other two data are Jamestown, the IVA iron with the lowest P and As values, and Obernkirchen, the IVA iron with the next lowest values; P values are based on electron-microprobe kamacite analyses by Reed (1969). Our preliminary SEM survey of three IVA irons having the lowest As contents revealed no P-rich phases, thus the bulk of the P appears to be in the kamacite. The P content of the taenite is several times lower than in kamacite but the amount of taenite is relatively small. To estimate bulk P contents we multiplied Reed's values by 0.98. We believe this to be conservative, and that the factor may be as low as 0.95.

Moore et al. (1969) and Lewis and Moore (1971) seem to have been near their detection limit, since they report their results to only one significant figure. It would be useful to have a new study of P in whole-rock iron meteorites and in their metallic phases.

Although there are only 12 IVA irons for which both P and As data are available (and only 3 other IVA irons for which P data determined by the milling technique studies), there is a large set of IIIAB data, and because IIIAB P concentrations are higher, the data are more precise, particularly at the low-Au end of the group (at the high-Au end large phosphides may have been under-sampled despite the use of milling).

Shown in Figure 4 are regression lines through the two data sets. We neglected the four IIIAB points that plot below the main trend at As values $> 10 \mu\text{g/g}$ (Owens Valley, Bald Eagle, Chupaderos, and Bella Roca); these irons have large troilite-schreibersite nodules, and it appears that the milling technique did not include representative amounts of these regions. The IVA irons Rembang (very low) and Duel Hill (slightly low but, because of its high Au, it has a moderate torqueing effect on the slope) were not included in the regression calculation. The IIIAB line has a slope of 1.20, the IVA line has a slope of 1.18. Within error, these slopes are the same. We suggest that P values calculated from As values and the IVA trend line: \log

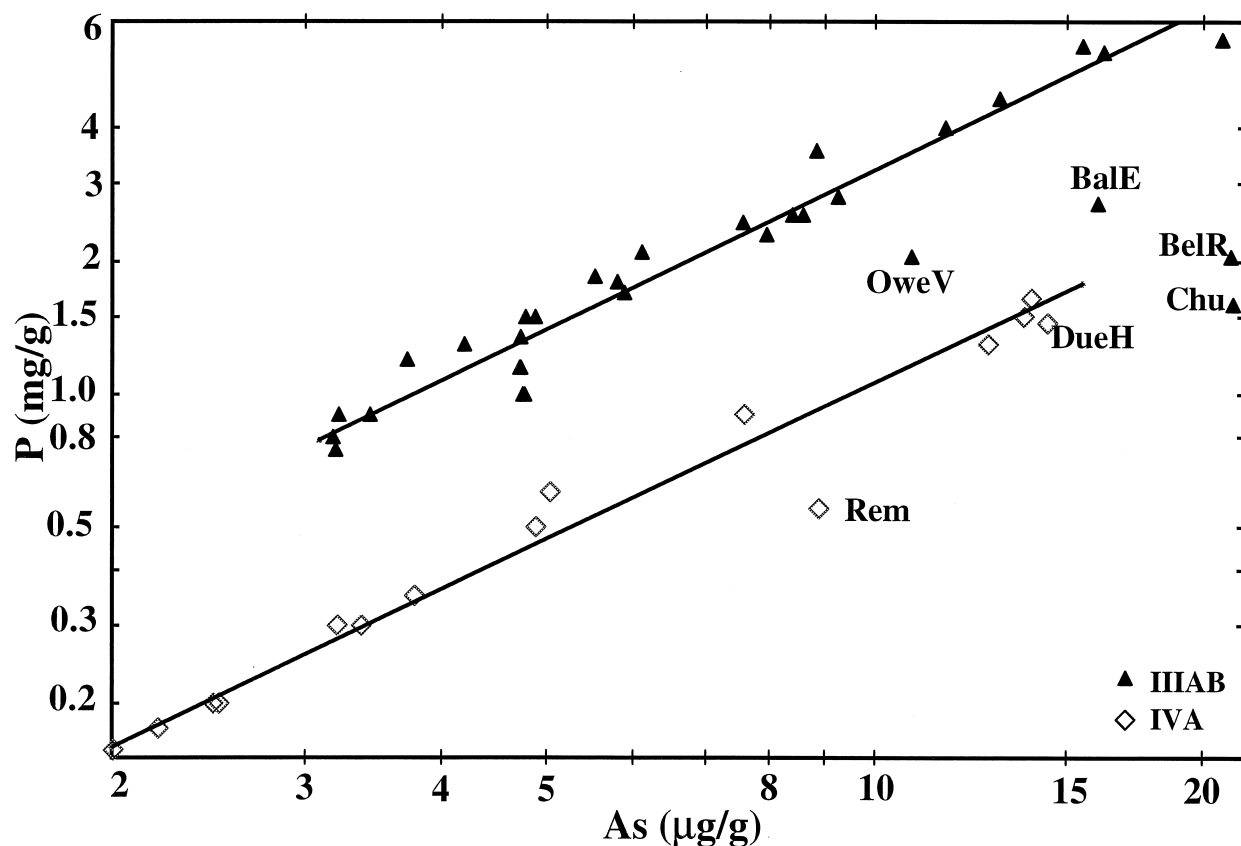


Fig. 5. The elements P and As are chemically similar in many settings, including fractionally crystallizing metallic cores. Here we plot whole-rock P data determined on milled samples of IIIAB and IVA irons (Moore et al., 1969; Lewis and Moore, 1971) against our As data for the metal. Some published P contents based on modal analysis of low-As IVA irons appear to be much too high; more accurate P contents can be calculated from a linear regression dependence of P on As. See text for details. Abbreviations: Bald Eagle (BalE), Bella Roca (BelR), Chupaderos (Chu), Duel Hill (DueH), Owens Valley (OweV) and Rembang (Rem).

$P = 1.178 \log As - 1.1508$ (where P is in mg/g and As in $\mu\text{g/g}$) are the best currently available estimates of IVA P data at low P concentrations.

The total range of IVA P values used by Rasmussen et al. (1995) extended from 0.4 to 1.8 mg/g. The 0.4 mg/g was for Yingde for which we calculate a P concentration of only 0.20 mg/g. The value of 1.8 mg/g was for Duchesne; it was obtained by Buchwald (1975) by point counting a relatively large section, and is probably equal or superior to the milled value of 1.5 mg/g (Moore et al. 1969). Thus the P values Rasmussen et al. used for high-Au IVA irons seem reasonably accurate.

7.3. Cooling Rates, Bandwidths, Nucleation Temperatures and the Density of Nuclei

We discussed above that the development of precise cooling-rate models requires accurate information about the $\alpha/(\alpha + \gamma)$ boundary, the Ni diffusion coefficients, and possibly the detailed nucleation mechanism. The effects of temperature and nonmetal content on these are poorly constrained at the low temperatures (≤ 850 K) where much of the development of the Widmanstätten pattern occurs.

In addition, the mean width of the kamacite bands depends

on the temperature at which kamacite nucleation occurs and the density of nuclei. The higher the nucleation temperature, the greater the rate of Ni diffusion, and, at a given spacing between nuclei, the thicker the resulting kamacite lamellae. And, the lower the density of nuclei, the greater the thickness kamacite lamellae can reach before parallel bands collide (impinge). After impingement occurs, further thickening of the kamacite can only be produced by the fusion of the impinging bands, but this requires that the intervening taenite lamella "dissolve" and the Ni be transported to other taenite regions. This process has occurred in a few slowly cooled irons, but the only driving force is the small difference in surface energy between the different taenite and kamacite regions, suggesting that the process is very slow, and may have rarely occurred in the IVA core.

The classic picture of kamacite nucleation is that this occurs homogeneously after undercooling of the metal some interval (say 100 K) below the $\gamma/(\alpha + \gamma)$ boundary. An alternative is that the kamacite nucleates heterogeneously on schreibersite that typically forms in the same general temperature interval (Moren and Goldstein, 1979).

We suggest that the simultaneous-nucleation scenario of

Schaudy et al. (1972) may help explain both the correlation of the estimated cooling rate with composition and the anomalously large variation in mean kamacite bandwidth and its correlation with composition. The starting assumption is that the IVA core had cooled well below the $\gamma/(\alpha + \gamma)$ boundary in all compositional regions and that an impact of the surface of the asteroid sent seismic waves through the core. If nucleation was initiated simultaneously throughout the body, it is plausible that the density of nuclei might have been proportional to the degree of undercooling, which was ≈ 50 K greater in low-Ni (74 mg/g) than in high-Ni (100 mg/g) irons. Thus the significant increase in bandwidth with increasing Au (Fig. 3) might be qualitatively explained by this model.

8. MODELING TRENDS IN GROUPS IVA AND IIIAB: PARTITION RATIOS, TRAPPED MELT

The IVA and IIIAB (Ir-Au) and (Ir-As) data are plotted together on Figures 6a,b; the two groups show very different trends. The IIIAB irons form a broad band with a high negative slope. The total Ir range in IIIAB is a factor of 2000 (the bottom end is not plotted) but only a factor of 31 in IVA. The IVA irons form a tight band with low negative slope in the beginning, but with the slope increasing to become roughly parallel to IIIAB in the lowest-Ir irons.

Wasson (1999) concluded that IIIAB compositions were the result of a combination of fractional crystallization and the incorporation of trapped melt; also shown on Figures 6a,b are the IIIAB solid and liquid tracks similar to those published by Wasson (1999) as well as solid and liquid tracks for IVA. In calculating these numerical tracks we allowed for the effects of increasing nonmetal contents (especially S) during the course of crystallization; more details are given below.

Laboratory studies (Jones and Drake, 1983; Jones and Malvin, 1990) show that Ir is highly compatible in crystallizing Fe-Ni metal (D_{Ir} values are always well above unity) whereas Au is incompatible, with D_{Au} less than 0.5 (D_{As} is not yet studied) at moderate S contents. Thus the irons having the highest Ir contents were the first to crystallize. D values for some elements are strongly dependent on the composition of the magma, particularly on its content of the nonmetallic elements S and P.

One can roughly estimate the S contents of magmas from irons that contain variable amounts of trapped melt; in group IIIAB Wasson (1999) estimated a S content of 20 mg/g (now revised up to 25 mg/g) by combining compositional data with S contents for Cape York irons differing in S content by a factor of 9. The amount of S in the IVA magma is difficult to evaluate, but FeS is less common and the typical large nodules appreciably smaller in IVA than in IIIAB. Wasson (1999) also estimated an initial S/P ratio of ≈ 4 g/g in the IIIAB magma. In most iron groups FeS is more abundant than schreibersite (roughly Fe_2NiP), and this is also true in group IVA. The P content of IVA metal is so low that, in the low-Au IVA irons, most remained dissolved in the metal; schreibersite contents are so low that Buchwald (1975) did not indicate their presence in his Appendix I. As discussed in more detail below, other volatile elements (e.g., Ga, Ge and Sb) were appreciably lower in the initial IVA magma than in the IIIAB magma.

Our initial D_{Ir} , D_{Au} and D_{As} values for IVA are 2.0, 0.25 and

0.14, respectively, substantially lower than initial IIIAB values published by Wasson (1999), 4.6, 0.38 and 0.30, respectively. One idea previously considered to explain the low range in Ir and the low Ir-Ni slope in group IVA was that, in this body inferred to be small based on its high cooling rate (in the previous section we suggest that it cooled at a rate 4X higher than IIIAB) equilibrium partitioning did not occur. This effect, which results from incomplete diffusion through boundary layers, would result in apparent D values closer to unity than the actual values. The fact that D_{As} and D_{Au} are much more extreme in IVA than in IIIAB shows that this model is incorrect. Jones and Drake (1983) and Jones and Malvin (1990) have shown that D_{Ir} and D_{Au} decrease as the S or P contents of metallic melts decrease. We therefore endorse the alternative model, that the content of nonmetals was much lower in the IVA magma than in the IIIAB magma, and that this resulted in the much lower D_{Ir} and D_{As} in this group.

We have attempted a simple model to allow for the dependence of D_{Ir} , D_{Au} and D_{As} on the S content. Jones and Malvin (1990) suggested that the best parameterization of such relationships would take the linear form:

$$\log D_E = A \cdot \log(1 - \alpha \cdot n \cdot X_N) + B \quad (1)$$

where D_E is the partition ratio of element E (in mol/mol), X_N is the mole fraction of nonmetal N in the metallic melt, n is sum of the moles of Fe and nonmetal in the stable solid and (i.e., 2 for S), and A, B, and α are constants obtained by trial fits of laboratory data. The Jones-Malvin model in effect assumes that there are two domains in the molten alloy, one dominated by the nonmetal and associated Fe, the other by other siderophiles including the Fe not associated with the nonmetal. This approach predicts relatively small changes in D_E at low X_N and very rapid change when $\alpha \cdot n \cdot X_N$ becomes larger (≥ 0.2).

In effect, the Jones-Malvin model assumes that short-range interactions between Fe and the nonmetal dominate molten ferrous alloy systems. If we accept the revised estimate of 25 mg/g S in the initial IIIAB, then the large change in D values (and particularly D_{Ir}) between lower S levels in group IVA and these IIIAB levels implies that even low S concentrations can profoundly affect D_{Ir} . As discussed below in connection with the curious IVA Cu-Au distribution, the contributions of different chemical interactions to the partition ratio may vary as the relative concentrations of the constituents evolve during the crystallization of the magma.

Wasson (1999) argued that the uncertainties in laboratory determinations of D Values are large enough to permit considerable latitude in choosing the relationship between these and nonmetal contents; he offered several arguments to justify this view (e.g., the very high concentrations of the "trace" elements in the experimental charges).

We followed the example of Wasson (1999) and examined the question of whether a simple relationship between D_E and nonmetal concentration could be used to generate a plausible fit to both the IIIAB and IVA Ir-Au and Ir-As trends with the only adjustable parameter being the initial composition of the magmas and the independent variable being the S content. For purposes of this simple test we did not attempt to incorporate the effects of P (which appears to be 3–4X less abundant than S in each group) on the system. We tried fitting both $\log D_E$ and

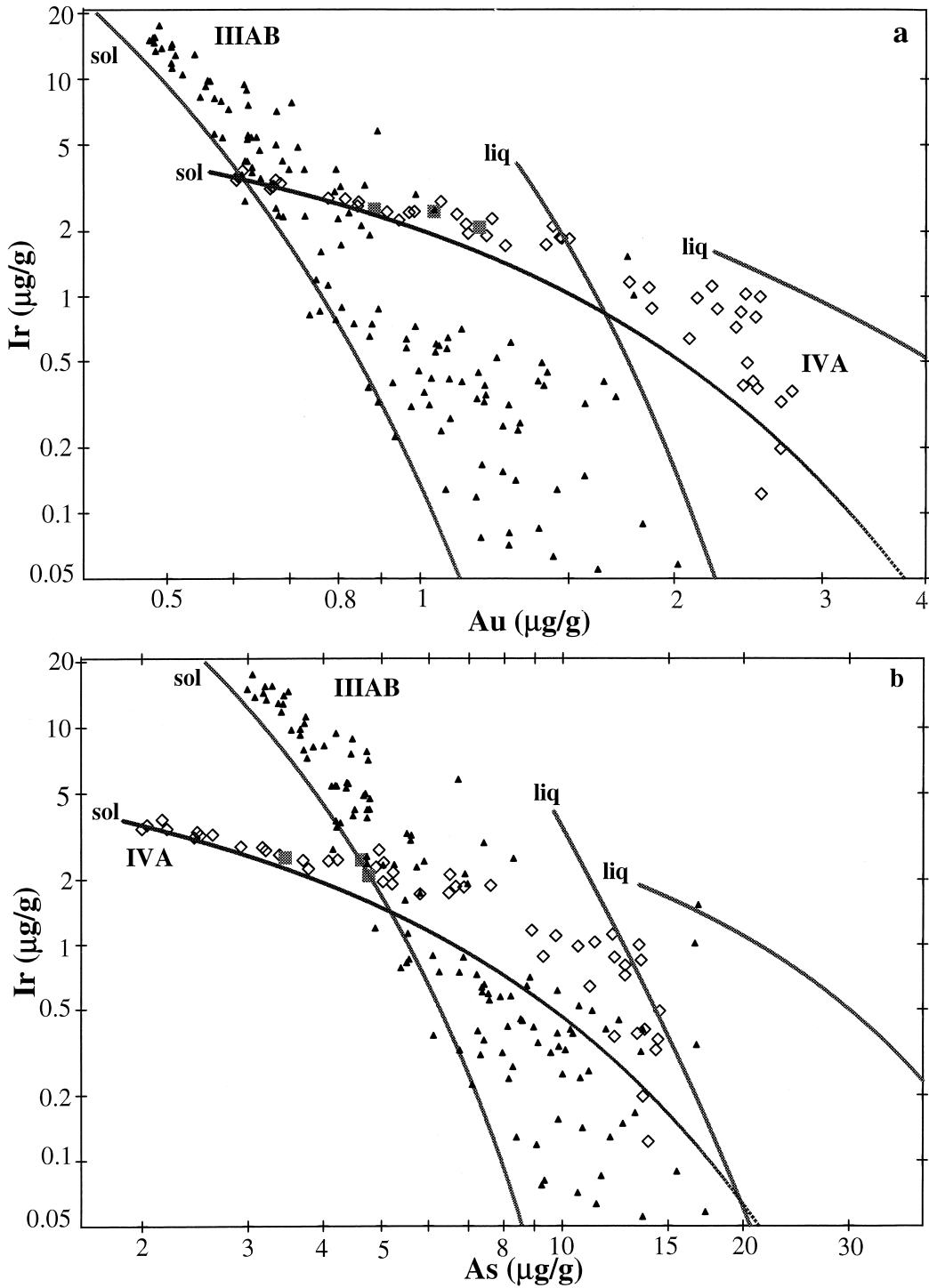


Fig. 6. On log-log (a) Ir-Au and (b) Ir-As diagrams IIIAB irons (small triangles) form a steeply negative trend, whereas IVA irons (open diamonds) form a trend that is initially shallow, but steepens at low Ir contents. Squares are extreme members of the Gibeon shower. Curves show calculated fractional-crystallization solid (sol) and liquid (liq) tracks based on an assumed quadratic relationship between D values and S (see text). IIIAB irons having Ir contents $< 0.05 \mu\text{g/g}$ are not shown.

D_E (in units of g/g) to linear and quadratic relationships with S concentration, and obtained our best fits with:

$$D_E = a \cdot S^2 + b \cdot S + c \quad (2)$$

where S is the concentration of S in mg/g and the constants are those listed in Table 2.

In Figure 6 we show the IVA and IIIAB fits we obtain from these constants on Ir-Au and Ir-As diagrams. We used a D_S

Table 2. Constants used in a quadratic fit of D_x values to S concentration inferred to be present in IVA and IIIAB irons: $D_E = a \cdot S^2 + b \cdot S + c$. Units of S in mg/g.

Element	a	b	c
As	$-2.85 \cdot 10^{-5}$	0.00507	0.119
Ir	$-9.10 \cdot 10^{-4}$	0.162	1.36
Au	$-1.85 \cdot 10^{-5}$	0.00378	0.0235

value of 0.005 and initial S contents of 4 mg/g in IVA and 25 mg/g in IIIAB. Of particular interest is how well the solid tracks fit the left margins of the fields, which we interpret to be samples with minimal contents of trapped melts. Our fits are satisfactory for this primitive approach, but algorithms leading to higher D_{Ir} values at S contents near the high end of IVA and the beginning of IIIAB would give better fits. We do not want to push the trial-and-error fitting farther until we have a better understanding of the chemical nature of the interaction of the nonmetals with Fe and with the trace metals. We will gain further insights into these questions with a detailed study of the third large magmatic group IIAB that is in progress.

During fractional crystallization the slope of the solid track on a log X-log Au diagram is equal to $(D_E - 1)/(D_{Au} - 1)$. We have estimated the initial slopes and intercepts by roughly fitting linear solid and liquid fractional crystallization tracks to the low-Au points on element-Au diagrams in Figures 1 and 2. We assumed that the Au content of the initial solid was 0.56 $\mu\text{g/g}$, as listed in Table 3. Because there are relatively high uncertainties associated with these fits we do not plot the tracks, but only list the inferred initial D values and intercepts in Table 3.

As discussed by Wasson (1999), irons such as Cape York with a wide range of trapped melt contents offer estimates of the S and P contents of the initial magma. In combination with modeling of the solid and liquid tracks, knowledge of the initial S content enables valuable tests of D values obtained by laboratory studies. Unfortunately, the number of sections of IVA irons large enough ($>200 \text{ cm}^2$) to permit modal estimation of S contents is small, but, as discussed above, future studies of large sections of Gibeon may permit such a direct evaluation of the IVA S content.

Table 3. Bulk composition of the IVA core estimated from the composition of the initial solids and the D values, and CI- and LL-normalized element/Ni and element/Au ratios.

Element (units)	Initial comp.	IVA D value	Bulk comp.	CI conc.	LL conc.	IIIAB/CI abund.	IVA/CI abund.	IVA/LL abund.
P ($\mu\text{g/g}$)	130	0.1	1300	1020	850	0.471	0.163	0.187
Cr ($\mu\text{g/g}$)	500	0.6	830	2650	3740	0.017	0.040	0.027
Co (mg/g)	3.79	0.95	3.99	0.508	0.49	1.283	1.008	0.996
Ni (mg/g)	72.2	0.88	83.4	10.7	10.2	$\equiv 1.000$	$\equiv 1.000$	$\equiv 1.000$
Cu ($\mu\text{g/g}$)	126	0.45	280	121	80	0.151	0.297	0.428
Ga ($\mu\text{g/g}$)	1.66	0.56	2.97	9.8	5.0	0.242	0.039	0.073
Ge ($\mu\text{g/g}$)	0.090	0.56	0.160	33	9	0.141	0.001	0.002
As ($\mu\text{g/g}$)	1.86	0.14	13.4	1.84	1.35	0.674	0.933	1.212
Sb (ng/g)	2	0.6	3.3	153	60	0.042	0.003	0.007
W (ng/g)	638	1.2	550	100	85	1.218	0.706	0.791
Re (ng/g)	340	2.0	200	37	33	1.260	0.693	0.741
Ir (ng/g)	3.75	1.99	1.88	0.46	0.36	1.140	0.525	0.639
Pt ($\mu\text{g/g}$)	6.35	1.4	4.70	0.99	0.85	1.036	0.610	0.677
Au ($\mu\text{g/g}$)	0.562	0.25	2.25	0.144	0.140	1.036	2.003	1.964

9. TRAPPED MELT IN GROUP IVA

On Figures 7a,b we show the IVA Ir-Au and Ir-As data together with mixing curves illustrating the effects of melt trapping. The IVA solid and liquid tracks are the same as shown in Figure 6, but we have now added mixing curves at degrees of crystallization of 0, 30, 50, 60, 70, 80 and 85%. The + signs on these curves mark 5% differences in the mix of equilibrium solids and liquids. We stress that the solid and liquid tracks are only rough approximations obtained (as discussed above) by trial-and-error filling of the IVA and IIIAB data, but we note that it is difficult to obtain fits, and that there is only a minor amount of freedom in choosing the parameters such as the initial D_{Au} , D_{Ir} , etc. Another potential complication in real cores is mixing between early solids and late liquids, which may have occurred in some cases; this would lead to mixing curves having higher mean (negative) slopes. Restricted by these caveats, the compositional Ir-Au data suggest that the maximum amount of trapped liquid is $\approx 30\%$, and the Ir-As data yield a maximum of $\approx 25\%$; the difference is well within the uncertainty of the method. If any of these IVA irons was produced by mixing earlier solids and later melts, the maximum amount of trapped liquid would be less than these values.

The best test of the interpretation of the trapped-melt, fractional-crystallization model would result from a detailed study of FeS abundances in IVA irons. We have initiated such a study, but have been frustrated by the rarity of large ($>200 \text{ cm}^2$) sections. As a result, we do not yet have enough data to provide a test. As noted above in the Gibeon discussion, compositional data and modal estimations of FeS need to be obtained on several large Gibeon sections to evaluate the relative contributions of these two processes, at least in this part of the IVA core.

10. VARIATIONS IN CU ACROSS GROUP IVA

As shown in Figure 1d, the Cu-Au trend in Group IVA is extraordinary. The trend is S shaped, passing through a maximum ($\approx 160 \mu\text{g/g}$ Cu) at about 1 $\mu\text{g/g}$ Au and a minimum ($\approx 110 \mu\text{g/g}$ Cu) at about 2 $\mu\text{g/g}$ Au before rising to 209 $\mu\text{g/g}$ Cu in Duel Hill (2.8 $\mu\text{g/g}$ Au). We know of no precedent for such a distribution.

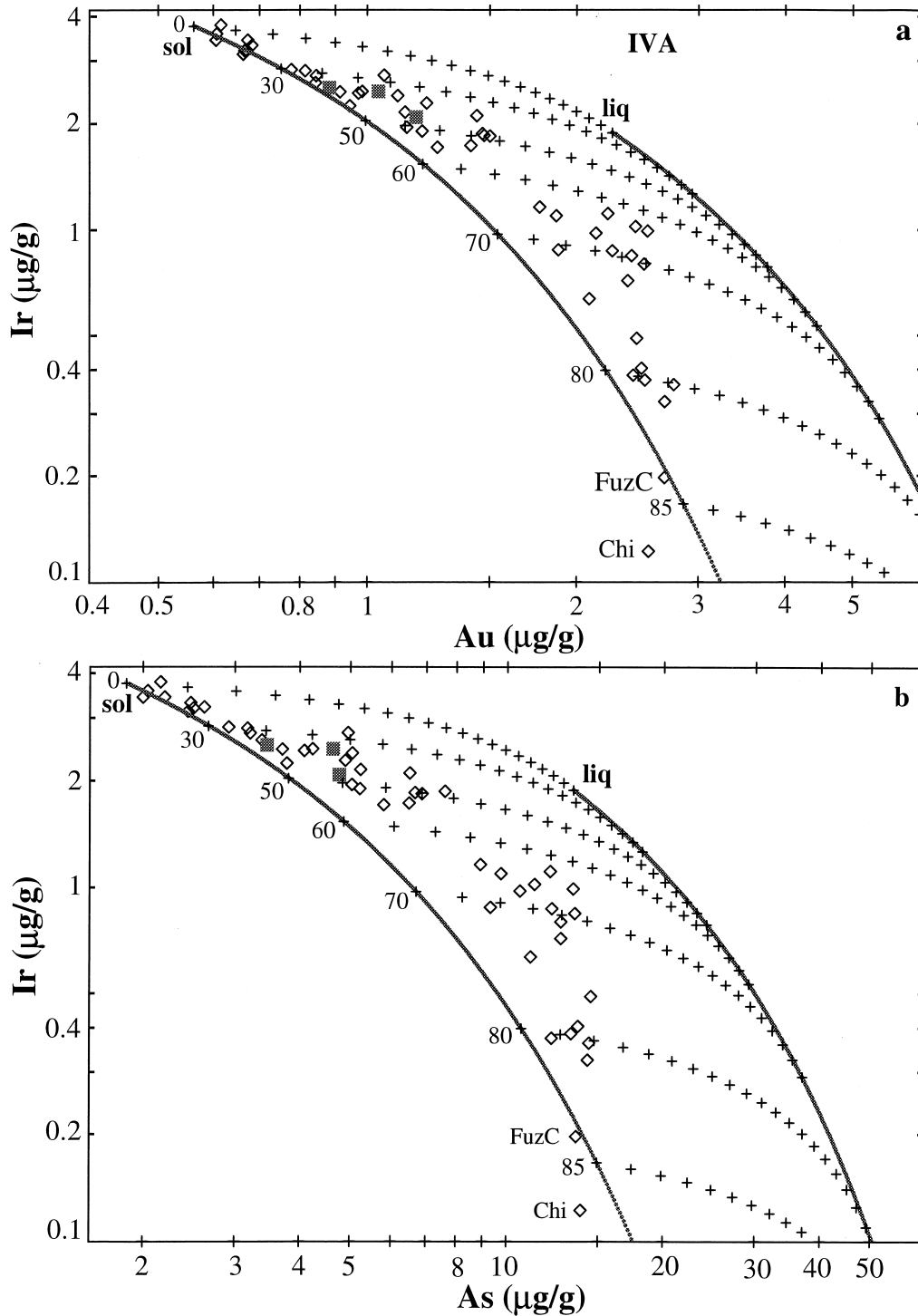


Fig. 7. Fractional crystallization and the effect of trapped melt are shown on log-log Ir-Au and Ir-As diagrams for our set of 48 IVA-irons. The solid and liquid tracks are those shown in Figure 6. Solid-liquid mixing trends are shown at indicated degrees of crystallization (in %) indicated by the numbers near the solid track. The model can account for all IVA irons except Chinaulta (Chi) which plots on the low-Au side of the field bounded by the solid-liquid tracks. The other low-Ir iron, Fuzzy Creek (FuzC) plots near our estimate of the solid tracks on both diagrams.

The IVA Cu distribution is quite different from that in IIIAB (note that, to enhance the clarity of Fig. 1d, the IIIAB points were multiplied by 1.5 before plotting). The IIIAB Cu-Au trend shows a low negative slope, with no clear evidence of sinuos-

ity. The vertical spread of the IIIAB distribution increases slightly with increasing Au content.

Because there are so many data and the replicates reproduce so well (numerous duplicate analyses are listed in the Appen-

dix), there is no doubt that this strange IVA Cu-Au trend is genuine. We considered two simple hypotheses to account for it: (1) The original distribution was largely flat; the trend is an artefact reflecting incomplete sampling of low-Cu IVA irons having Au in the range 0.7 to 1.0 $\mu\text{g/g}$ and high-Cu irons in the Au range 1.7 to 2.2 $\mu\text{g/g}$. (2) The trend reflects changes in D_{Cu} from <1 at Au $<0.9 \mu\text{g/g}$ to >1 at Au between 1 and 2 $\mu\text{g/g}$ to <1 at Au $> 2.2 \mu\text{g/g}$.

There are two problems with the first hypothesis (a) if large parts of the IVA core are unsampled, this should produce noticeable gaps in trends involving other elements, and (b) this stochastic-sampling model requires regional (as opposed to meter-scale) variations in Cu that are unrelated to Au, and there is no obvious way to produce these.

The changes in D_{Cu} required for the second hypothesis are similar to but more complex than those required to explain the Ga-Au and Ge-Au trends in IIIAB and IVA. The latter pass through maxima, thus implying the D values gradually change from <1 to >1 . What is then needed for the Cu is another change that is unprecedented, one that would make Cu again start to be incompatible. As a cartoon of what might be the answer, the first solid to crystallize might be the bcc δ phase, in which the Cu might be somewhat incompatible. After a minor amount of crystallization the γ phase began to crystallize, and the Cu may have become compatible. Later, when the S content of the melt became high enough, the Cu might have switched again, perhaps because of sulfide complexes forming in the melt. This cartoon would be more believable if the final, high-Au trend were the same as observed in the low-Au IIIAB irons that seem to have similar nonmetal contents. There is, at most, a hint that the initial slope of the IIIAB Cu-Au trend is positive.

11. MEAN ELEMENTAL ABUNDANCES IN THE IVA CORE; FRACTIONATION OF VOLATILE SIDEROPHILES

We can use the method of Scott (1977) to estimate the bulk composition of the IVA core from the composition of the first solid to crystallize and from the solid/liquid partition ratios (D values) derived by rough linear fits to the low-Au irons that appear to lie close to the solid crystallization track. We list these values in Table 3 together with CI- and LL-normalized element/Ni ratios. The approach requires that we know (or assume) the D value of one element; we assumed that the initial D_{Au} inferred from our modeling, 0.250, was correct. We normalized these abundances to Ni rather than Au because this is the practice followed in the past and because D_{Ni} is much closer to unity than is D_{Au} , thus minimizing possible compositional effects resulting from melt trapping. We also list tentative CI-normalized element/Ni ratios for group IIIAB. These will be reexamined and revised when we publish our extensive set of IIIAB data, but we expect most changes to be minor, $<20\%$. We note that significant fractions of two elements, Cr and P, may have remained in the mantle as oxides during the extraction of metal to form the core, and that minor fractions of Ga and Ge may also have formed mantle oxides.

Elements that are refractory during nebular condensation show systematic variations among the chondrite groups. The highest Si- or Mg-normalized refractory lithophile abundances (1.4X CI) are found in the CV chondrites, the lowest in the

enstatite (EH and EL, $0.6\times$ CI) chondrites. Refractory siderophile data show similar variations if normalized to Ni rather than Mg or Si. The best determined refractory in our IVA set of elements is Ir and its abundance is low relative to CI chondrites (Table 3). This suggests a relationship to the ordinary or enstatite chondrites, but firm links require the IVA Au/Ir fractionation (discussed below) to be understood. In contrast the Ir abundance is high in IIIAB relative to CI chondrites, similar to those observed in carbonaceous chondrites (other than CI or CR). As mentioned in the introduction, the O-isotopic composition observed in IVA silicates is similar to that in L and LL ordinary chondrites, and that for IIIAB is below the terrestrial-fractionation (TF) line, and to this degree is similar to carbonaceous chondrites other than CI. Because of the links suggested by the O-isotope composition, we also normalize the IVA abundances to LL chondrites, which also have the highest Au/Ir ratios among the OC.

The IVA irons show large depletions in S and the most volatile siderophiles. Is this volatile depletion the result of parent-body or nebular processes? Perhaps the strongest evidence that chondritic asteroids have lost volatile elements is found in the L-chondrite data of Tandon and Wasson (1968); the highest In contents in L3 chondrites are $200\times$ higher than in L6 chondrites. Studies of Pb, Tl and Cd show similar trends (e.g., Keays et al., 1971). The lower volatile contents of the type 4 to 6 chondrites are generally attributed to losses that occurred during thermal metamorphism on the parental asteroid. The source of the heat is not clear. There is reason to doubt that enough ^{26}Al was present in the OC parent bodies to produce the required temperature increase (Kita et al., 2000). We favor the Rubin (1995) view that metamorphic heating was mainly produced by impacts. Whatever the heat source, it would seem that a more intense version of the same asteroidal processes could have raised temperatures to levels leading to the loss of Ge, Sb, Ga and As from the IVA iron meteorite parental materials.

Scott et al. (1996) argued that volatile loss could not be the result of impact heating. Their main argument against impact melting of a chondrite parental material is: "impact melts should contain abundant cool clasts and cool rapidly." In our opinions, this statement is only correct for surficial cratering events on a low-porosity body. If asteroidal bodies collide at 5 km s^{-1} , there is enough energy released to melt a large fraction of the projectile and the target. If the large body was porous (and the first generation of nebular planetesimals must have had porosities $\gg 50\%$), it is plausible that much of the energy could have been converted to heat, and that the resulting melt could have been covered by a thick, insulating layer. If the viscosities were low, the metallic magma would have separated from the silicates. The impact portion of this model is mechanically similar to the Haack et al. (1996) fragmentation-reassembly model.

Returning to the remarkably low IVA Ir/Au ratio ($\approx 0.3\times$ CI), we have examined three possible models that could generate this ratio from a chondritic parental material. In all three the fractionation is largely attributed to the large difference between the D_{Au} and D_{Ir} solid/liquid ratios; this difference is so large (we infer an initial IVA $D_{\text{Au}}/D_{\text{Ir}} \approx 0.13$) that a partial melt extracted from a chondritic parent would have a Ir/Au ratio $\approx 7\times$ lower than that in the parent.

The three possible models we have considered are: (1) the high-Ir irons were the first solids to crystallize from a chondritic (in terms of siderophiles) parental magma, but were not equilibrium solids, but mixtures of solid and trapped melt; (2) the terrestrial set of IVA irons is grossly incomplete, with no irons from the first half of the core to crystallize; and (3) the high-Ir irons were the first solids to crystallize, they were equilibrium solids containing minimal amounts of trapped melt, but the initial magma was not chondritic because of incomplete melting of the chondritic metal during core formation.

The trapped-melt model can explain the high Ir/Au ratio if the high-Ir irons consist of a roughly 50:50 mixtures of solid and trapped melt. This has the effect of raising the resulting Au content by about 50% and lowering the Ir content by $\approx 40\%$, roughly the factors needed to make the magmatic Au/Ir ratio chondritic. This model predicts that low-Au, high-Ir IVA irons should contain moderate fractions of FeS. However, the three irons having the highest Ir contents are relatively small, and it is possible that even a 50% trapped melt might not be obvious in these small irons. On the other hand, it does not seem plausible that, on a scale of ≈ 1 m (set by diffusional mixing), that all 7 irons at the high-Ir ($>3.2 \mu\text{g/g}$) end of group IVA would contain $\geq 50\%$ trapped melt without this having been recognized. In fact, Buchwald (1975) examined a moderate size section ($\approx 200 \text{ cm}^2$) of one of these, Yanhuatlan, and estimated the S content to be only 0.4 mg/g , too low to allow 50% trapped melt even if initial S content of the magma was only 4 mg/g , our best estimate. We conclude that this is not a viable model.

We used numerical modeling to determine the degree of fractional crystallization required to reduce the Ir/Au ratio of the initial-liquid by a multiplicative factor of 0.3 required to produce the ratio (Table 3) in the parental liquid of the high-Ir irons from an LL chondrite initial liquid. Using the model shown in Figure 6, we find that 52% crystallization is needed to produce the observed values in the pure solid, and 42% crystallization if the high-Ir irons are assumed to consist of 90% solids and 10% trapped melt. Although not aesthetically pleasing that such a large fraction of the IVA core is unsampled, we have not found a strong argument against this model.

The third model seems more plausible because there is reason to believe that metal in chondritic asteroids is generally incompletely melted during core formation. However, the amount of residual, unmelted metal still has to be relatively high, on the order of 50% of that originally present. Metallic melts form over a wide range of temperatures ranging from the metal-FeS eutectic near 1260 K to complete melting of low-FeS metal near 1770 K . Incomplete melting can occur because the separation of immiscible melts occurs as soon as viscosities in the metal and silicates drop to levels low enough to permit segregation. After the upward segregation of a plagioclase-rich silicate melt and the downward segregation of a S-rich metallic melt it is unlikely that enough additional heat can be generated in the residual solids (which are much more refractory than the original chondritic solids) to permit a second separation ("milk-ing") of metallic melt.

A reviewer (NC) noted that the low S content we use for IVA would lead to a melting temperature very near that of the pure solid, and that this model implies that the composition of the IVA core was very sensitive to the heat input. From the Fe-S

phase diagram (Brandes and Brook, 1992) we estimate that 4 mg/g S would lower the melt temperature by $\approx 14 \text{ K}$ relative to the pure solid. We note, however, that olivine melts in the same temperature interval, and that the presence of this and the unmelted metal had a thermostating effect. Thus, increasing the amount of injected heat by 10% would probably not have resulted in complete melting of the metal.

The above description of melt separation particularly applies if a "slow" heat source, e.g., ^{26}Al decay, produced the first milking; separation of metal and silicate occurred when the degree of melting reached a critical value, and some, perhaps most of the heat source migrated into surficial regions. If the heat source was "rapid" e.g., compressive heating during impacts, all the melting would occur during a very short interval, and no additional heat is liberated to fuel a second extraction of a metallic melt. One cannot, however, rule out a second impact.

Impact melting tends to produce melts that are depleted in refractories (Widom et al., 1986) and analysis of magnetic separates of ordinary chondrites (e.g., Chou et al., 1973; Rambaldi et al., 1978) showed that an appreciable fraction of these are trapped in silicates, and thus might not have entered a metallic melt formed by impact. Thus, the depletion of Ir in the initial IVA melt may in part be the result of non-equilibrium processes association with impact heating.

12. SUMMARY

We report concentrations of 12 elements in IVA iron meteorites. Group IVA is one of the three large magmatic groups that show clear compositional evidence of fractional crystallization. A comparison of our IVA data with those for IIIAB, the largest magmatic group, shows that solid liquid distribution coefficients (D values) were substantially lower in IVA, resulting in much lower slopes on Ir-Au and Ir-As diagrams. With the possible (but, we argue, unlikely) exception of the first-crystallized part of the IVA core, the terrestrial set of IVA and IIIAB irons seems to include representatives from essentially all parts of the original cores. Interestingly, although Ir shows a much larger total fractionation in IIIAB (factor of 2000 vs. 30 in IVA), As is more fractionated in IVA (factor of 7 vs. 6 in IIIAB). The lower D values in IVA are attributed to low S contents compared to IIIAB; we roughly estimate that the initial IVA S content was 4 mg/g , $6\times$ lower than that in IIIAB. Such a low S content is consistent with the low contents of other volatile elements such as Ga, Ge and Sb. Wasson (1999) argued that the compositions of IIIAB irons imply large amounts of trapped melt; IVA irons also show evidence of melt trapping, but average fractions are appreciably lower.

The low volatile contents of IVA iron meteorites may have affected the development of the Widmanstätten pattern. Most past attempts to estimate IVA cooling rates from the kamacite-taenite system yielded relatively high rates that correlate with composition. Such a correlation is inconsistent with the irons having all cooled within a single core (or other mass of metal). Suggestions that the correlation could be real, and the result of breakup and reassembly of the parent asteroid (and its core), seem contrived and implausible. We suggest that there remains enough latitude in the laboratory data to permit phase boundaries and diffusion coefficients that lead to cooling rates that are independent of composition. Another interesting possibility is

that, because there was too little P to permit schreibersite formation at high (ca. 1000 K) temperatures, the IVA materials were able to cool well below the $\gamma/(\alpha + \gamma)$ boundary without kamacite nucleation, and that this must be incorporated into future cooling-rate models. We note that there are several indicators of near-constant cooling rates within IVA including the very similar kamacite compositions profiles in low-Ni and high-Ni irons and the similar sizes of the taenite islands in cloudy taenite across the IVA compositional spectrum.

Acknowledgments—We thank Finn Ulff-Møller, Byeon-Gak Choi and Eric Jerde for assistance in gathering the INAA data. Constructive reviews were contributed by N. Chabot, H. Haack and an anonymous reviewer; those by Chabot and Haack were detailed and led to many changes, some major. K. Rasmussen kindly calculated a number of kamacite and taenite profiles for us. A number of curators provided samples, often on relatively short notice; within the past five years we received IVA specimens from R. S. Clarke and T. McCoy of the Smithsonian Institution, G. Kurat of the Naturhistorisches Museum, Vienna, C. B. Moore of Arizona State University, M. Prinz of the American Museum, M. Grady and S. A. Russell of The Natural History Museum, London, M. Wadhwa of the Field Museum, and M. E. Zucolotto of the Museu Nacional, Rio de Janeiro. We also received IVA samples from V. F. Buchwald, M. Cilz, J. Hyman, B. Reed and S. Schoner. First-rate technical support was kindly provided by S. Yoo and S. Zhang. This research was mainly supported by NASA grant NAG5 to 4331.

Associate editor: H. Palme

REFERENCES

- Brandes E. A. and Brook G. B. (1992) *Smithells Metal Reference Handbook*, pp. 11–269. Butterworth-Heinemann.
- Buchwald V. F. (1975) *Handbook of Iron Meteorites*. Univ. California Press.
- Clayton R. N. and Mayeda T. K. (1996) Oxygen isotope studies of achondrites. *Geochim. Cosmochim. Acta* **60**, 1999–2017.
- Dean D. C. and Goldstein J. I. (1986) Determination of the interdiffusion coefficients in the Fe-Ni and Fe-Ni-P systems below 900°C. *Metall. Trans.* **17A**, 1131–1138.
- Esbensen K. H., Buchwald V. F., Malvin D. J., and Wasson J. T. (1982) Systematic compositional variations in the Cape York iron meteorite. *Geochim. Cosmochim. Acta* **46**, 1913–1920.
- Goldstein J. I. and Short J. M. (1967) Cooling rates of 27 iron and stony-iron meteorites. *Geochim. Cosmochim. Acta* **31**, 1001–1023.
- Graham A. L., Bevan A. W. R., and Hutchison R. (1985) *Catalogue of Meteorites*. Univ. of Arizona Press.
- Haack H. and Scott E. R. D. (1992) Asteroid core crystallization by inward dendritic growth. *J. Geophys. Res.* **97**, 14727–14734.
- Haack H., Scott E. R. D., Love S. G., and Brearley A. (1996) Thermal histories of IVA stony-iron and iron meteorites: Evidence for asteroid fragmentation and reaccretion. *Geochim. Cosmochim. Acta* **60**, 3103–3113.
- Hills J. G. and Goda M. P. (1998) Damage from the impacts of small asteroids. *Planet. Space Sci.* **46**, 219–229.
- Hirano K., Cohen M., and Averbach B. L. (1961) Diffusion of nickel into iron. *Acta Metall.* **9**, 440–445.
- Jones J. H. and Drake M. J. (1983) Experimental investigations of trace element fractionations in iron meteorites: II: The influence of sulfur. *Geochim. Cosmochim. Acta* **47**, 1199–1209.
- Jones J. H. and Malvin D. J. (1990) A nonmetal interaction model for the segregation of trace metals during solidification of Fe-Ni-S, Fe-Ni-P, and Fe-Ni-S-P alloys. *Metall. Trans.* **21b**, 697–706.
- Keays R. R., Ganapathy R., and Anders E. (1971) Chemical fractionations in meteorites-IV. Abundances of fourteen trace elements in L-chondrites; implications for cosmochemistry. *Geochim. Cosmochim. Acta* **35**, 337–363.
- Kita N. T., Nagahara H., Togashi S., and Morishita Y. (2000) A short duration of chondrule formation in the solar nebula: Evidence from ^{26}Al in Semarkona ferromagnesian chondrules. *Geochim. Cosmochim. Acta* **64**, 3913–3922.
- Lewis C. F. and Moore C. B. (1971) Chemical analyses of thirty-eight iron meteorites. *Meteoritics* **6**, 195–205.
- Malvin D. J., Wang D., and Wasson J. T. (1984) Chemical classification of iron meteorites-X. Multielement studies of 43 irons, resolution of group IIIE from IIIAB, and evaluation of Cu as a taxonomic parameter. *Geochim. Cosmochim. Acta* **48**, 785–804.
- Moore C. B., Lewis C. F., and Nava D. (1969) Superior analyses of iron meteorites. In *Meteorite Research* (ed. P. M. Millman), pp. 738–748. Reidel.
- Moren A. E. and Goldstein J. I. (1978) Cooling rate variations of group IVA iron meteorites. *Earth Planet. Sci. Lett.* **40**, 151–161.
- Moren A. E. and Goldstein J. I. (1979) Cooling rate of group IVA iron meteorites determined from a ternary Fe-Ni-P model. *Earth Planet. Sci. Lett.* **43**, 151–161.
- Rambaldi E. R., Cendales M., and Thacker R. (1978) Trace element distribution between magnetic and non-magnetic portions of ordinary chondrites. *Earth Planet. Sci. Lett.* **40**, 175–186.
- Rasmussen K. L., Ulff-Møller F., and Haack H. (1995) The thermal evolution of IVA iron meteorites: Evidence from metallographic cooling rates. *Geochim. Cosmochim. Acta* **59**, 3049–3059.
- Reed S. J. B. (1969) Phosphorus in meteoritic nickel-iron. In *Meteoritic Research* (ed. P. M. Millman), pp. 749–762. Reidel.
- Reisener R. J. and Goldstein J. I. (2000). Experimental studies of taenite decomposition in ordinary Chondrites during continuous cooling (abstract). *Meteorit. Planet. Sci.* **35**, A135–A136.
- Romig A. D. and Goldstein J. I. (1980) Determination of the Fe-Ni and Fe-Ni-P phase diagram at low temperatures (700°C to 300°C). *Metall. Trans.* **11A**, 1151–1159.
- Rubin A. E. (1995) Petrologic evidence for collisional heating of chondritic asteroids. *Icarus* **113**, 156–167.
- Saikumar V. and Goldstein J. I. (1988) An evaluation of the methods to determine the cooling rates of iron meteorites. *Geochim. Cosmochim. Acta* **52**, 715–726.
- Schaudy R., Wasson J. T., and Buchwald V. F. (1972) The chemical classification of iron meteorites-VI. A reinvestigation of irons with Ge concentrations lower than 1 ppm. *Icarus* **17**, 174–192.
- Scott E. R. D. (1972) Chemical fractionation in iron meteorites and its interpretation. *Geochim. Cosmochim. Acta* **36**, 1205–1236.
- Scott E. R. D. (1977) Geochemical relationships between some pallasites and iron meteorites. *Mineral. Mag.* **41**, 265–272.
- Scott E. R. D., Haack H., and McCoy T. (1996) Core crystallization and silicate-metal mixing in the parent body of the IVA iron and stony-iron meteorites. *Geochim. Cosmochim. Acta* **60**, 1615–1631.
- Tandon S. N. and Wasson J. T. (1968) Gallium, germanium, indium and iridium variations in a suite of L-group chondrites. *Geochim. Cosmochim. Acta* **32**, 1087–1110.
- Wasson J. T. (1999) Trapped melt in IIIAB irons; solid/liquid elemental partitioning during the fractionation of the IIIAB magma. *Geochim. Cosmochim. Acta* **63**, 2875–2889.
- Wasson J. T., Choi B.-G., Ulff-Møller F., and Jerde E. (1998) Chemical classification of iron meteorites: XII. New members of the magmatic groups. *Geochim. Cosmochim. Acta* **62**, 715–724.
- Wasson J. T. and Kallemeyn G. W. (1988) Compositions of chondrites. *Philos. Trans. R. Soc. London* **A325**, 535–544.
- Wasson J. T., Lange D. E., Francis C. A., and Ulff-Møller F. (1999) Massive chromite in the Brenham pallasite and the fractionation of Cr during the crystallization of asteroidal cores. *Geochim. Cosmochim. Acta* **63**, 1219–1232.
- Widom E., Rubin A. E., and Wasson J. T. (1986) Composition and formation of metal nodules and veins in ordinary chondrites. *Geochim. Cosmochim. Acta* **50**, 1989–1995.
- Willis J. and Wasson J. T. (1978a) Cooling rates of group IVA iron meteorites. *Earth Planet. Sci. Lett.* **40**, 141–150.
- Willis J. and Wasson J. T. (1978b) A core origin for Group IVA iron meteorites: A reply to Moren and Goldstein. *Earth Planet. Sci. Lett.* **40**, 162–167.
- Yang C.-W., Williams D. B., and Goldstein J. I. (1997) A new empirical cooling rate indicator for meteorites based on the size of the cloudy zone of the metallic phases. *Meteorit. Planet. Sci.* **32**, 423–429.

APPENDIX

Table A1. Replicate analyses of IVA irons carried out at UCLA in 1986 and later.

Meteorite	dt yr.	Cr μg/g	Co mg/g	Ni mg/g	Cu μg/g	Ga μg/g	As μg/g	W μg/g	Re ng/g	Ir μg/g	Pt μg/g	Au μg/g
Altonah	99	64	3.96	82.7	136	2.08	7.61	0.49	193	1.88	5.5	1.44
Altonah	99	170	3.95	86.5	141	2.19	7.57	0.49	213	1.86	5.0	1.48
Alvord	86	46	3.97	84.8	127	1.97	6.50	0.49	210	2.05		1.40
Alvord	86	71	3.99	90.6	132	2.47	6.50	0.57	280	2.17		1.50
Alvord	00	59	3.97	83.8	112	2.00	6.49	0.58	247	2.09	5.2	1.42
Bishop Canyon	00	324	3.90	77.1	153	2.08	2.90	0.59	362	2.85	5.5	0.78
Bodaibo	00	185	3.91	78.3	147	2.25	3.85	0.56	265	2.24	6.6	0.93
Bodaibo	00	186	3.91	77.6	146	2.36	3.71	0.60	276	2.24	4.7	0.94
Boogaldi	99	58	4.12	88.1	109	2.35	10.9	0.39	57	0.63	5.4	2.05
Boogaldi	99	62	4.09	91.0	107	2.40	11.3	0.45	64	0.63	4.4	2.11
Bristol	99	137	3.92	79.1	129	2.14	5.13	0.53	228	1.95	6.4	1.14
Bristol	99	140	3.93	79.5	131	2.13	4.92	0.55	222	1.94	5.5	1.13
Bushmanland	99	31	4.02	89.8	116	2.27	9.64	0.48	126	1.14	4.9	1.87
Bushmanland	99	260	4.04	84.1	115	2.34	9.84	0.42	110	1.05	7.1	1.86
Chinaulta	93	49	4.21	97.3	133	1.85	14.1	0.29	<29	0.12	2.6	2.48
Chinaulta	93	44	4.25	93.5	127	2.11	13.6	0.27	<19	0.11	3.1	2.58
Cleburne	86	19	4.07	87.9	124	2.38	7.17	0.53	210	1.83	6.8	1.47
Cleburne	86	125	3.98	88.1	135	2.27	6.56	0.57	220	1.86	6.7	1.53
Cranberry Plains	00	21	4.19	94.9	141	2.36	13.5	0.40	121	0.97	5.5	2.49
Cratheus	00	246	3.92	80.3	141	2.04	3.80	0.57	274	2.42	7.0	0.97
Duchesne	99	96	4.16	91.7	121	2.04	13.7	0.35	29	0.40	3.0	2.49
Duchesne	99	12	4.14	93.6	125	2.14	13.7	0.30	33	0.40	2.5	2.46
Duel Hill (54)	93	35	4.30	104	200	2.14	13.9	0.28	35	0.37	<3.4	2.69
Fuzzy Creek	00	17	4.31	108	150	2.06	13.0	0.33	<30	0.21	2.9	2.59
Gan Gan	98	23	4.17	91.3	118	2.43	12.3	0.44	120	1.10	4.8	2.20
Gan Gan	99	22	4.08	92.2	114	2.28	11.8	0.42	113	1.11	5.1	2.22
Gibeon (King)	95	246	3.82	81.0	161	2.32	3.75	0.63	330	2.64	7.5	0.88
Gibeon 3748	97	374	3.86	78.9	161	2.20	3.95	0.58	300	2.41	5.7	0.93
Gibeon 3758	93	219	3.88	74.8	153	2.29	3.29	0.55	251	2.49		0.86
Gibeon 3758	97	228	3.86	79.8	162	1.78	3.39	0.60	316	2.55	6.2	0.88
Gibeon 3761	93	184	3.87	76.9	176	2.08	3.52	0.72	277	2.52		0.89
Gibeon 3761	97	2299	3.77	79.6	183	2.01	3.62	0.55	294	2.51	5.5	0.88
Gibeon 3762	93	215	3.88	82.7	172	1.84	4.75	0.75	269	2.58		1.05
Gibeon 3762	97	207	3.88	81.1	173	2.34	4.77	0.72	303	2.64	5.1	1.06
Gibeon 3777	93	181	3.89	81.2	160	2.23	4.54	0.59	263	2.34		1.01
Gibeon 3777	97	270	3.88	82.7	158	2.22	4.26	0.56	290	2.36	6.6	1.01
Harriman (Of)	99	138	3.93	79.1	126	2.10	5.05	0.52	200	1.91	5.2	1.19
Harriman (Of)	99	132	3.94	84.5	129	2.15	5.36	0.48	199	1.89	5.5	1.20
Hill City	96	45	4.09	87.5	115	2.13	10.7	0.41	<40	0.97	5.3	2.12
Hill City	96	48	4.09	88.0	108	2.48	10.5	0.41	120	0.97	4.1	2.13
Huizopa	99	166	3.86	79.0	157	2.04	3.46	0.60	294	2.59	5.0	0.84
Huizopa	99	186	3.91	76.1	154	2.01	3.29	0.54	301	2.60	5.1	0.83
Jamestown	00	337	3.86	73.1	132	1.74	2.06	0.59	411	3.49	7.7	0.59
Kossuth	96	52	4.15	92.3	126	2.54	12.2	0.40	180	0.88	7.6	2.27
Kossuth	96	57	4.12	93.0	117	2.50	12.1	0.34	70	0.85	4.3	2.22
La Grange	99	221	3.90	75.4	163	2.19	3.17	0.61	306	2.73	5.5	0.83
La Grange	99	224	3.87	76.9	160	1.96	3.24	0.59	327	2.70	6.1	0.85
Mantos Blancos	99	74	4.03	86.6	104	2.35	9.20	0.43	89	0.86	4.3	1.87
Mantos Blancos	99	71	4.06	88.1	108	2.29	9.38	0.44	83	0.88	4.7	1.88
Maria da Fe	98	411	3.79	74.3	134	1.73	2.14	0.62	453	3.78	6.8	0.61
Maria de Fe	99	413	3.75	74.6	144	1.63	2.18	0.62	483	3.77	7.5	0.61
Maria Elena	99	335	3.83	73.0	144	1.68	2.37	0.63	351	3.41	5.8	0.68
Maria Elena	99	340	3.84	77.0	150	2.08	2.57	0.61	372	3.20	5.2	0.67
Mart	99	25	4.16	95.4	118	2.32	12.6	0.38	67	0.71	4.1	2.38
Mart	00	24	4.18	91.3	114	2.28	12.8	0.35	61	0.71	3.9	2.35
Mount Sir Chas	00	136	3.95	81.6	124	2.36	5.95	0.52	198	1.80	5.0	1.25
Muonionalusta	92	107	3.93	86.5	115	2.10	6.67	0.53	198	1.73	5.6	1.42
Muonionalusta	00	93	4.03	82.0	110	2.07	6.09	0.49	177	1.72	4.7	1.36
Muonionalusta ^b	92	86	3.90	88.9	137	2.16	7.50	1.98	186	1.76	6.0	1.48
Muonionalusta ^b	92	99	3.93	89.6	134	2.46	7.50	2.25	179	1.77	5.6	1.49
Namibia 1999 ^a	99	157	3.94	76.6						2.13	5.6	1.19
Namibia 1999 ^a	99	133	3.93	81.7	134	1.98	4.74	0.55	247	2.08	6.6	1.18
Namibia 1999 ^a	00	131	3.97	80.7	122	2.06	4.77	0.52	242	2.07	5.2	1.17

(Continued)

Table A1. Continued

Meteorite	dt yr.	Cr $\mu\text{g/g}$	Co mg/g	Ni mg/g	Cu $\mu\text{g/g}$	Ga $\mu\text{g/g}$	As $\mu\text{g/g}$	W $\mu\text{g/g}$	Re ng/g	Ir $\mu\text{g/g}$	Pt $\mu\text{g/g}$	Au $\mu\text{g/g}$
New Westville	99	26	4.11	93.3	110	2.54	14.6	0.27	24	0.48	4.2	2.44
New Westville	99	56	4.15	95.3	116	2.26	14.4	0.32	49	0.49	5.7	2.43
Ningbo	00	106	3.99	79.5	125	2.04	5.24	0.58	247	2.26	5.1	1.12
Obernkirchen	99	530	3.85	79.9	147	1.97	2.25	0.61	423	3.40	6.6	0.66
Obernkirchen	99	534	3.85	77.8	145	1.69	2.15	0.69	390	3.46	5.1	0.67
Otchinjau	99	161	3.90	77.5	157	2.00	4.20	0.55	286	2.44	4.3	0.99
Otchinjau	99	169	3.89	79.3	163	2.15	4.25	0.83	268	2.48	5.4	0.97
Page City	97	74	4.18	95.2	121	2.07	14.0	0.22	25	0.32	3.8	2.58
Page City	97	17	4.25	95.8	123	2.09	14.6	0.25	29	0.32	4.0	2.77
Para de Minas	99	157	3.93	80.4	146	2.24	5.13	0.57	268	2.38	6.0	1.10
Rembang	99	72	4.03	85.4	112	2.24	8.85	0.47	115	1.16	4.4	1.78
Rembang	00	65	4.03	88.4	108	2.37	8.93	0.46	110	1.16	4.3	1.75
San Franc. Mtns	99	362	3.85	76.3	162	2.24	3.07	0.67	351	2.83	6.0	0.81
San Franc. Mtns	99	357	3.85	79.4	164	1.98	3.26	0.58	331	2.78	6.1	0.81
São João Nepo.	99	31	3.88	80.2	161	2.09	4.90	0.55	326	2.71	5.5	1.05
São João Nepo.	99	30	3.90	80.4	163	2.14	4.99	0.53	318	2.74	5.8	1.05
Seneca Twnshp.	92	79	4.45	83.6	109	2.28	6.19	0.55	232	1.73	6.3	1.38
Seneca Twnshp.	95	94	3.88	84.4	117	2.40	7.10	0.54	226	1.97	5.2	1.56
Signal Mtn.	99	194	3.89	77.4	142	2.11	3.73	0.53	270	2.45	4.9	0.91
Signal Mtn.	99	174	3.88	76.9	148	2.07	3.66	0.56	271	2.45	5.4	0.90
Smithland	99	101	4.14	91.1	131	2.21	13.7	0.36	82	0.84	4.2	2.39
Smithland	99	116	4.12	89.8	122	2.19	13.3	0.37	80	0.84	3.6	2.40
Social Circle	99	485	3.81	72.3	130	1.63	2.07	0.61	424	3.57	5.6	0.61
Social Circle	99	463	3.78	70.9	127	1.80	2.01	0.59	402	3.57	6.2	0.59
Steinbach	91	36	4.20	98.7	170	2.13	12.7	0.43	90	0.86	4.6	2.41
Western Ark.	99	342	3.85	77.4	151	1.98	2.67	0.65	396	3.24	5.7	0.66
Western Ark.	99	301	3.82	76.9	149	1.67	2.57	0.65	383	3.19	6.1	0.67
Wood's Mtn.	99	94	3.91	83.2	159	2.17	4.78	0.58	265	2.26	3.7	1.19
Wood's Mtn	99	82	3.90	83.2	156	2.23	5.00	0.63	260	2.30	5.3	1.24
Yanhuitlan	99	363	3.84	76.6	155	2.01	2.59	0.61	403	3.24	6.7	0.66
Yanhuitlan	99	781	3.82	73.9	145	1.86	2.40	0.64	368	3.16	6.4	0.66
Yindge	00	400	3.86	76.0	146	1.77	2.45	0.63	372	3.24	6.5	0.65

^a We suspect Namibia 1999 to be a sample of Gibeon.

^b These samples of Muonionalusta IV appear to be contaminated with W. Because of heavy etching they may also have elevated taenite/kamacite ratios.

Table A2. Sources and catalog numbers of the samples.

Meteorite	Source	Cat. no.	Meteorite	Source	Cat. no.	Meteorite	Source	Cat. no.	Meteorite	Source	Cat. no.
ALH A78252	AMC	78252,5	Duel Hill 1854	UCLA	634	Mart	FMNH	me1040	San Franc. Mtn	SI	1270
Altonah	SI	863	Fuzzy Creek	UCLA	1474	Millarville	UCLA	1025	São João Nepo	SI	6881
Alvord	SI	6286	Gan Gan	UCLA	1477	Mt. Sir Charles	SI	5669	Seneca Twnshp	SI	1325
Bishop Canyon	FMNH	1955	Gibeon	VFB	see text	Muonionalusta	RMS	460054	Signal Mountn	AMNH	866
Bodaído	UCLA	1169	Harriman (Of)	SI	6072	Namibia 1999	UCLA	1478	Smithland	HarU	148
Boogaldi	NHML	86924	Hill City	SI	1436	New Westville	SI	1412	Social Circle	SI	1675
Bristol	UCLA	591	Huizopa	UCLA	665	Ningbo	UCLA	1074	Steinbach	UCLA	755
Bushmanland	SI	2515	Jamestown	HarU	558	Obernkirchen	SI	987	Western Arkans	SI	794
Chinaulta	NHM	1913,434	Kossuth	UCLA	1390	Otchinjau	NHML	1953,61	Wood's Mountn	SI	717
Cleburne	UCLA	1207	La Grange	UCLA	247	Page City	UCLA	1406	Yanhuitlan	FMNH	962
Cranberry Plns	HarU	197C	Mantos Blancos	NHML	53323	Para de Minas	NMR	108mt	Yingde	UCLA	1102
Cratheus 1931	NHML	1931,254	Maria da Fe	NMR	63mt	Rembang	GMB	1525			
Duchesne	UCLA	144	Maria Elena	SI	1221	Rica Aventura	FMNH				

Abbreviations of the sources: AMC, Antarctic Meteorite Committee; AMHN, American Museum of National History; FMNH, Field Museum of Natural History; GMB, Geological Museum, Batavia; HarU, Harvard University; NHML, The Natural History Museum, London; NMR, National Museum, Rio; RMS, Rijksmuseet Stockholm; SI, Smithsonian Institution; UCLA, University of California, Los Angeles.

A3. Questions About Pairing

In general, our data set shows relatively few cases where pairing might be suspected. For example, Social Circle and Jamestown have almost identical compositions, but the reported discovery locations are >1500 km apart, thus pairing seems to be excluded.

The Gibeon shower discussed above has provided many thousands of meteorites to the world, and it is inevitable in cases such as this that some of these would make their way into collections under incorrect place names. It is interesting to note that there are several meteorites that are essentially unresolvable from one or the other of the three Gibeons in our set. These are readily recognized in Figs. 7a,b, and with more effort, in Figs. 1 and 2 (two points represent Gibeon specimens from the Windhoek pile, the high-Au point the specimen we call Namibia 1999. The names of the meteorites having both Au concentrations in the range 0.86–1.20 $\mu\text{g/g}$ and Ir values in the range 2.04–2.56 are: Bodaibo, Cratheus (1931), Ningbo, Otchinjau, Para de Minas and Signal Mountain. Of these, only Otchinjau (from Angola) is reported to be from a region near Namibia. We suggest that Otchinjau should be treated as a specimen of Gibeon until evidence to the contrary is reported. Wasson et al.

(1998) discussed the fact that we suspect Albion to be a mislabeled specimen of Gibeon, mainly because it appeared on the market just as the mineral shows were being flooded with Gibeon specimens, and no adequate field research (such as interviews with the original discoverer) have ever been reported.

E. Zucolotto (pers. comm. 1999), suspects that Cratheus (1931) is a mislabeled piece of the 116-kg Para de Minas mass. Although their compositions are as closely related as the extreme specimens of Gibeon, they are more different than we expect from materials that were separated by a maximum of about 40 cm, thus we think they should be treated as separate falls until more compositional, isotopic or structural data have become available that support pairing them. Interestingly, another Brazilian IVA iron, the silicate-rich São João Nepomuceno, is closely related to these compositionally. It was not listed with the Gibeon-like irons because its Ir (2.73 $\mu\text{g/g}$) is slightly higher than the stated range. The reported discovery locations of Para de Minas and São João Nepomuceno are about 300 km apart.